**RESEARCH ARTICLE**

# Vps13 is required for timely removal of nurse cell corpses

Anita I. E. Faber[1], Marianne van der Zwaag[1], Hein Schepers[1], Ellie Eggens-Meijer[1], Bart Kanon[1], Carmen IJsebaart[1], Jeroen Kuipers[1], Ben N. G. Giepmans[1], Raimundo Freire[2,3,4], Nicola A. Grzeschik[1], Catherine Rabouille[1,5] and Ody C. M. Sibon[1,*]

## ABSTRACT

Programmed cell death and consecutive removal of cellular remnants is essential for development. During late stages of *Drosophila melanogaster* oogenesis, the small somatic follicle cells that surround the large nurse cells promote non-apoptotic nurse cell death, subsequently engulf them, and contribute to the timely removal of nurse cell corpses. Here, we identify a role for Vps13 in the timely removal of nurse cell corpses downstream of developmental programmed cell death. Vps13 is an evolutionarily conserved peripheral membrane protein associated with membrane contact sites and lipid transfer. It is expressed in late nurse cells, and persistent nurse cell remnants are observed when Vps13 is depleted from nurse cells but not from follicle cells. Microscopic analysis revealed enrichment of Vps13 in close proximity to the plasma membrane and the endoplasmic reticulum in nurse cells undergoing degradation. Ultrastructural analysis uncovered the presence of an underlying Vps13-dependent membranous structure in close association with the plasma membrane. The newly identified structure and function suggests the presence of a Vps13-dependent process required for complete degradation of bulky remnants of dying cells.

KEY WORDS: Vps13, Programmed cell death (PCD), Oogenesis, Endoplasmic reticulum, Death cell degradation, Membrane contact sites

## INTRODUCTION

During development and tissue remodelling, excessive or unnecessary cells undergo programmed cell death (PCD). The most extensively studied form of PCD is apoptosis, which involves the activation of caspases. Apoptosis is characterized by condensation of chromatin, nuclear fragmentation and membrane blebbing (Kerr et al., 1972). Other forms of PCD include necrosis and autophagic cell death, of which the involved mechanisms and players are only starting to be unravelled (Chen et al., 2018; Gudipaty et al., 2018; Mohammadinejad et al., 2018; Tait et al., 2014). Cell death can be triggered in a cell autonomous as well as cell non-autonomous manner by surrounding cells (Brown and

Neher, 2014, 2012; Pérez-Garijo et al., 2013; Tait et al., 2014; Wilson et al., 2009). In both cases, cell death is followed by the efficient clearance of the dead cell remnants. This is required for homeostasis of the organism, and lack of this clearance has been linked to multiple human diseases, including chronic obstructive pulmonary disease (COPD), atherosclerosis and cancer (Poon et al., 2014), underscoring the importance of this process.

Both PCD and subsequent clearance of remnants of dying cells also play an important role during late stages of oogenesis in *Drosophila melanogaster*. *Drosophila* females have two ovaries, each containing a series of tubular ovarioles in which the egg chambers develop (Verheyen and Cooley, 1994) (Fig. 1A,B). Egg chambers consist of 16 germline cells, including 15 nurse cells and 1 oocyte, which are surrounded by a layer of somatically derived follicle cells. The individual egg chambers are produced by germline and somatic stem cells in the germarium, after which they grow through 14 well-defined developmental stages (Verheyen and Cooley, 1994). During the first stages of oogenesis, nurse cells produce nutrients that are transferred into the oocyte cytoplasm through ring canals. At stage 10B-11, the nurse cells deposit their entire cytoplasm in the oocyte in a process called 'cytoplasmic dumping'. This is followed by the initiation of developmental PCD. Subsequent removal of dying nurse cells occurs via a process driven by the surrounding follicle cells which form membrane expansions that engulf the nurse cell debris (Giorgi and Deri, 1976; Nezis et al., 2000; Serizier and McCall, 2017; Tran and Berg, 2003). Failure of either developmental PCD or impairment of clearance by follicle cells leads to accumulation of persistent nurse cell nuclei during the last stages of oogenesis (Peterson et al., 2015).

Little is known about the triggers and the nature of nurse cell PCD during late stages of *Drosophila* oogenesis. It is considered to be non-apoptotic as caspases do not play a major role (Baum et al., 2007; Foley and Cooley, 1998; Mazzalupo and Cooley, 2006; Peterson et al., 2003). Autophagy has been thought to play a role in the induction of nurse cell death because it leads to the degradation of the apoptotic inhibitor Bruce, thereby potentially allowing cell death triggering (Nezis et al., 2010). However, autophagy and caspases only play a minor role in PCD during oogenesis. Indeed, combined inhibition of autophagy and caspases does not largely interfere with developmental PCD (Peterson and McCall, 2013), suggesting the presence of other inducers of cell death. The engulfing follicle cells surrounding the late oogenesis nurse cells play a role in inducing nurse cell PCD, because PCD is prevented upon genetic ablation of these follicle cells (Timmons et al., 2016). Moreover, the specific downregulation of the engulfment gene *draper* in engulfing follicle cells results in impaired DNA fragmentation of nurse cell nuclei, which is an early marker of induced cell death (Timmons et al., 2016). In addition, the phagocytic gene *Ced-12*, integrins and genes associated with lysosomal function and intracellular trafficking are factors expressed in follicle cells that are involved in the subsequent removal of nurse cells (Timmons et al., 2017, 2016). This indicates

[1]Department of Biomedical Sciences of Cells and Systems, University Medical Center Groningen, The University of Groningen, 9713 AV, Groningen, The Netherlands. [2]Unidad de Investigación/FIISC, Hospital Universitario de Canarias, Ofra s/n, La Cuesta, 38320 San Cristóbal de La Laguna, Tenerife, Spain. [3]Instituto de Tecnologías Biomédicas, Universidad de La Laguna, 38200 San Cristóbal de La Laguna, Tenerife, Spain. [4]Facultad de Ciencias de la Salud, Universidad Fernando Pessoa Canarias, 35450 Las Palmas de Gran Canaria, Spain. [5]Hubrecht Institute, University of Utrecht, 3584 CT, Utrecht, The Netherlands.

*Author for correspondence (o.c.m.sibon@umcg.nl)

C.I.-J., 0000-0002-0009-6829; O.C.M.S., 0000-0002-6836-6063

DEVELOPMENT

1
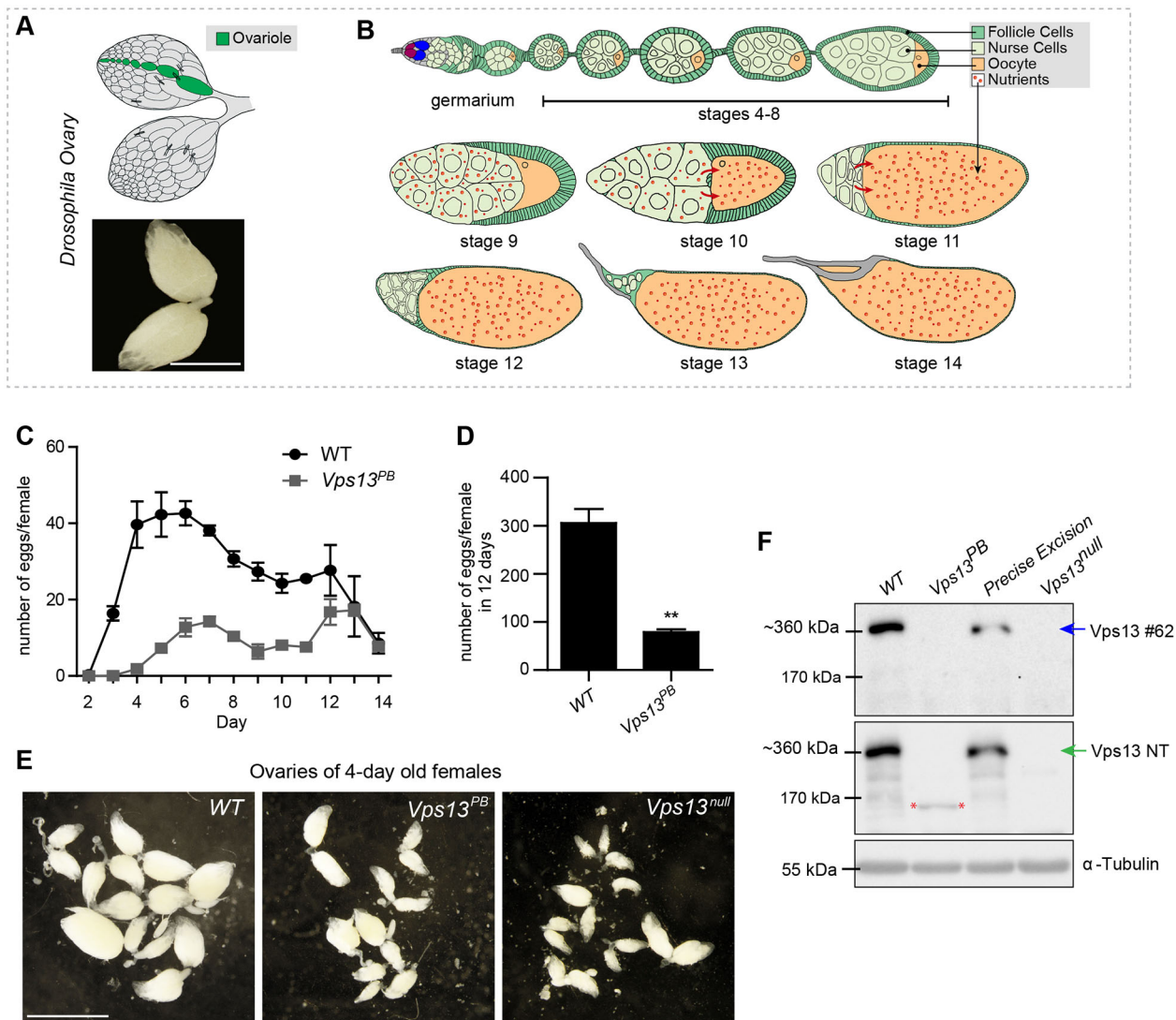
**Fig. 1. *Vps13* mutants have a reduced fecundity.** (A) Upper image: schematic of *Drosophila* oogenesis. Lower image: dissected paired ovaries from wild-type females. The paired ovaries each contain a series of tubular ovarioles in which the egg chambers develop; an individual ovariole is indicated in green, earlier stages on the left and mature stages on the right. Scale bar: 0.5 mm. (B) Various stages of oogenesis. Egg chambers consist of 16 germline cells, including 15 nurse cells and 1 oocyte. The germline cells are surrounded by a layer of somatically derived follicle cells. The individual egg chambers are produced by germline and somatic stem cells in the germarium, after which they grow through 14 well-defined developmental stages. During the first stages of oogenesis, nurse cells produce nutrients that are transferred into the oocyte cytoplasm through ring canals. At stage 10-11, the nurse cells deposit their entire cytoplasm in the oocyte in a process called cytoplasmic dumping. Developmental PCD is initiated and removal of dying nurse cells occurs. (C,D) Egg lay capacity of wild-type (WT) and *Vps13$^{PB}$* mutant flies was recorded for indicated days. The average number of eggs laid per female per day is shown (C) and total egg production is quantified (D). **$P<0.01$ (two-tailed unpaired Student's *t*-test). (E) Dissected ovaries of 4-day-old female wild type, *Vps13$^{PB}$* and *Vps13$^{null}$* mutants. Scale bar: 1 mm. (F) Western blot analysis of Vps13 levels in control (wild type and precise excision line) and *Vps13* mutant ovaries using the Vps13 #62 (upper panel) and Vps13 NT (lower panel) antibodies. Arrows indicate the band representing the full length Vps13 protein, migrating around 360 kDa, asterisks indicate the truncated Vps13 protein present in the *Vps13$^{PB}$* mutant. Tubulin staining was used as a loading control.

a major role for engulfing follicle cells in the timely removal of nurse cell remnants. These data support a model in which follicle cells are required to: (1) induce nurse cell death; (2) provide lysosomes that invade the nurse cell remnants and cause acidification of the nuclear remnants, activating nurse cell DNAse-II activity and DNA degradation; and (3) engulf the nurse cell corpses. All in concert, this contributes to the efficient removal of the remnants (Bass et al., 2009; Mondragon et al., 2019; Timmons et al., 2017, 2016; Yalonetskaya et al., 2020).

In contrast to the role of follicle cells and follicle cell-derived factors, nurse cell autonomous roles and factors involved in the removal of nurse cells are relatively unknown. Here, we demonstrate

that the peripheral membrane protein Vacuolar protein sorting 13 homolog (Vps13), the *Drosophila* orthologue of human VPS13A, is expressed in nurse cells and is required for the timely removal of nurse cell corpses during late oogenesis. VPS13-family members are multitasking proteins playing important roles in membrane formation, membrane contact sites and lipid transfer (Bean et al., 2018; Kumar et al., 2018; Lang et al., 2015; Nakanishi et al., 2007; Park et al., 2013; Park and Neiman, 2012; Xue et al., 2017; Yeshaw et al., 2019). Information of the possible *in vivo* functions of VPS13 proteins so far has been obtained by overexpression studies, tagged VPS13 proteins and investigating VPS13-depleted phenotypes. No localization studies of endogenous VPS13 proteins are yet

present. Mutations in the human *VPS13A* gene lead to the rare autosomal recessive neurodegenerative disease Chorea-Acanthocytosis (ChAc), which is characterized by neurodegeneration and the presence of acanthocytes (spiky red blood cells) (Danek and Walker, 2005; Rampoldi et al., 2001; Ueno et al., 2001). We have previously reported that *Vps13 Drosophila* mutants show a neurodegenerative phenotype upon ageing (Vonk et al., 2017). While characterizing the phenotype of *Drosophila Vps13* mutant flies, we observed a significant accumulation of persistent nurse cell nuclei in mutant ovaries and, here, investigated this in detail. Our results provide evidence for a Vps13-dependent structure and function for the timely clearance of large remnants of superfluous cells downstream of PCD and acidification.

## RESULTS
### *Vps13* mutants have a reduced fecundity
Previously, we have reported that insertion of a piggyBac transposable element in the *Vps13* gene (*Vps13^{PB}*) leads to a neurodegenerative phenotype in *D. melanogaster* (Vonk et al., 2017). Upon further examination we noticed that homozygous female *Vps13^{PB}* mutants produced fewer offspring compared with wild-type flies, and a significant delay and reduction in egg laying was observed (Fig. 1C,D). Accordingly, homozygous *Vps13^{PB}* females contained smaller ovaries compared with wild-type females (Fig. 1E). This suggests a specific role for Vps13 in ovary development and/or homeostasis. Western blot analysis using an antibody against the C-terminal domain of Vps13 (Vonk et al., 2017) (Vps13#62) revealed the presence of full-length Vps13 protein in extracts of wild-type ovaries (Fig. 1F, Fig. S1A). In agreement with the ovary phenotype, full-length Vps13 was below detection levels in ovary extracts from *Vps13^{PB}* homozygous mutants. Conversely, an antibody against the N-terminal domain (Vps13NT; Fig. S1A) detected a truncated protein in the mutant extract (Fig. 1F). The presence of an N-terminal-containing truncated part of Vps13 in lysates of ovaries from *Vps13^{PB}* homozygous mutants is in agreement with the position of the piggyBac insertion (Fig. S1A) and is consistent with Vps13 western blot analysis of samples derived from homozygous *Vps13^{PB}* fly heads (Vonk et al., 2017). Precise excision of the piggyBac element (hereafter called 'precise excision'; Excision line 1 from Vonk et al., 2017) restored the levels of full-length Vps13 protein in ovary extracts (Fig. 1F).

The presence of a truncated Vps13 product in the *Vps13* mutant could lead to a toxic gain-of-function, potentially obscuring the interpretation of the mutant phenotype. Therefore, we created a protein-null *Vps13* mutant using CRISPR/Cas9 (Bassett and Liu, 2014; Dominguez et al., 2016; Housden et al., 2014; Sander and Joung, 2014). A *Vps13* knockout mutant was generated by targeting exon 4 and exon 8 at the N terminus of the *Vps13* gene (Fig. S1A). Potential mutant lines were analyzed by western blot using antibodies recognizing either the Vps13 N or C terminus and a null mutant was searched for that expresses neither the full-length protein nor an N terminus fragment. One of the lines fulfilled these characteristics, hereafter called *Vps13^{null}* (Fig. 1F). Sequencing revealed a 2 bp deletion in exon 8 (Fig. S1A), leading to a premature stop codon and the absence of the Vps13 protein in this *Vps13^{null}* mutant (Fig. 1F).

Analysis of *Vps13^{null}* mutant ovaries showed a similar size reduction as the *Vps13^{PB}* mutant when compared with wild types (Fig. 1E). The number of eggs per female was also reduced in the *Vps13^{null}* mutant and in *Vps13^{null/PB}* transheterozygous females (Fig. S1B). Furthermore, qPCR analysis of the *Vps13^{null}* showed a significant reduction in *Vps13* mRNA when compared with an isogenic CRISPR/Cas9 control line harbouring no mutations in the *Vps13* gene (CC control) (Fig. S1C). Consistent with Vonk et al., *Vps13^{null}* mutants also showed a reduced lifespan (Fig. S1D).

Thus, the *Vps13^{null}* CRISPR/Cas9 mutant is a validated *Vps13^{null}* mutant that can be used in addition to the *Vps13^{PB}* mutant to investigate the role of Vps13 during oogenesis. The similarities between the two independently generated *Vps13* mutants further underscore that the phenotypes are caused by loss of Vps13 function and are not due to the genetic background.

### *Vps13* mutant ovaries show an accumulation of persistent nurse cell nuclei
We next investigated the ovaries of wild-type, *Vps13^{null}* and *Vps13^{PB}* mutant females in more detail, and a 'persistent nurse cell nuclei' phenotype (PNCN) was observed in *Vps13* mutants. After dumping cytoplasm from the nurse cells into the oocyte compartment, the nurse cells undergo PCD and are fully removed and further degraded in a follicle cell-dependent manner (Nezis et al., 2000). When removal of the nurse cell remnants is impaired, PNCN is observed (visualized by staining with DAPI) (Peterson et al., 2015; Timmons et al., 2016). When compared with wild types, ovaries of the two independently generated *Vps13* mutants exhibited a significant increase of stage-14 egg chambers containing one or more PNCN at the final stage of oogenesis (stage 14) (Fig. 2A-C). Consistently, ovaries derived from Vps13^{null/PB} transheterozygous females showed a comparable phenotype. The amount of PNCN per stage-14 egg chambers, when positive, was on average 2-3, indicating that most nurse cell nuclei are degraded in time in the mutants (Fig. 2D). Compared with previously published mutants harbouring a PNCN phenotype including *draper* (Etchegaray et al., 2012), the *Vps13* mutants displayed a mild phenotype. This mild PNCN phenotype is associated with mutations in *Vps13*, but is most likely not the only explanation for the small ovaries and the decreased fecundity of *Vps13* homozygous mutant females.
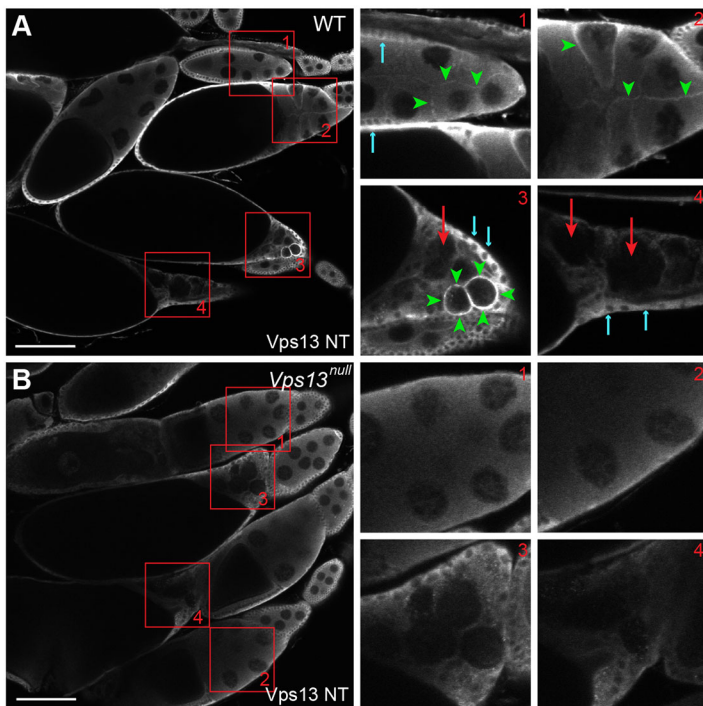
### Vps13 protein is in close association with the boundaries of individual nurse cells and enriched in late stages of oogenesis
Next, we aimed to immunolocalize Vps13 protein in ovaries. Immunofluorescence staining of wild-type ovaries with the Vps13 NT antibody (Vonk et al., 2017) revealed a signal during stage 4-10 of oogenesis corresponding to nurse cell boundaries (Fig. 3A, green arrowheads in boxed areas 1 and 2). A more distinct and intense ring-shaped expression pattern, again reminiscent of the shape of boundaries of individual nurse cells, was observed at stage 11-12 of oogenesis, when nurse cell size becomes smaller owing to cytoplasmic dumping (Fig. 3A, green arrowheads in boxed area 3; Fig. S2A,B, white arrows). At this stage, nurse cell degradation starts and these degrading nurse cells can clearly be distinguished from non-degrading ones, at earlier stages, by their intense non-homogeneous and irregular-shaped DAPI staining, characteristic for nuclei undergoing cell death (Fig. S2A,B, asterisks) (Bass et al., 2009; Kerr et al., 1972; Nezis et al., 2006; Timmons et al., 2016; Yalonetskaya et al., 2020). Nurse cells in a more advanced degradation stage are associated with a less pronounced Vps13 signal (Fig. 3A, red arrows in boxed areas 3 and 4; Fig. S2A,B, asterisk 3). This suggests that the intense nurse cell Vps13 ring-like signal at stage 11-12 is transient. In addition, a more diffuse staining was also visible in the surrounding follicle cells (Fig. 3A, blue arrows) at all stages. Importantly, the distinct Vps13-positive pattern

**Fig. 2. *Vps13* mutant ovaries show an accumulation of PNCN.** (A) Schematic representation of a normal stage-14 egg chamber and a stage-14 egg chamber with PNCN in light green. (B) Stage-4 egg chambers of wild-type (WT), *Vps13*$^{PB}$ and *Vps13*$^{null}$. Nuclei and PNCN are visualized by DAPI staining. Pyknotic PNCN are indicated by the green arrows. Scale bar: 50 μm. (C) Quantification of the percentage of stage-14 egg chambers containing PNCN in WT, the precise excision control line, *Vps13*$^{PB}$, *Vps13*$^{null}$ and *Vps13*$^{null}$/*Vps13*$^{PB}$ transheterozygous flies. ****$P<10^{-6}$ (Fisher's exact test). ns, not significant. (D) Dot plot analysis visualizing the amount of PNCN per stage-14 egg chamber that contained PNCN. Each symbol represents one stage-14 egg chamber that is positive for PNCN. On the *y*-axis the number of PNCN per egg chamber is given. Stage-14 egg chambers positive for PNCN of WT, the precise excision control line, *Vps13*$^{PB}$, *Vps13*$^{null}$ and *Vps13*$^{null}$/*Vps13*$^{PB}$ transheterozygous flies were analysed.

associated with the nurse cells was absent in *Vps13*$^{null}$ and *Vps13*$^{PB}$ ovaries (Fig. 3B; Figs S2D and S3), demonstrating the specificity of the Vps13 signal in the nurse cells, whereas the signal observed in the follicle cells is likely non-specific as it is also visible in *Vps13*$^{null}$ and *Vps13*$^{PB}$ ovaries.

To investigate Vps13 localization in nurse cells with a non-immunobased approach (Schnell et al., 2012), we engineered a fly line expressing a 3′ tagged Vps13-GFP fusion at the endogenous locus using the CRISPR/Cas9 system, (Fig. S4A,B,D). The *Vps13-GFP* fly line is viable, no significant increase in PNCN was detected, and their life span was similar to wild-type flies (Fig. S4C,E), indicating that the *Vps13-GFP* fusion protein is functional. *Vps13-GFP*-expressing ovaries showed a similar pattern that overlapped with the Vps13 NT antibody staining corresponding to the nurse cell boundaries, enriched in stage 11-12 (Fig. S2C).

## Downregulation of Vps13 in the nurse cells, but not in follicle cells, leads to the accumulation of PNCN

The prominent localization pattern of Vps13 associated with nurse cells of late oogenesis (Fig. 3) could be associated with the nurse cells themselves, but also could represent Vps13 present in follicle cells that have migrated and have invaded with long small protrusions between nurse cells at that stage (Nezis et al., 2000; Serizier and McCall, 2017; Timmons et al., 2016; Tran and Berg,

2003). To investigate this, we specifically downregulated Vps13, either in the germ line cells (including the nurse cells), using the *nanos*-GAL4 driver or in follicle cells using the *GR1*-GAL4 driver to express RNA interference (RNAi) constructs to downregulate Vps13. The specificity of the follicle and germ cell drivers was demonstrated by combining them with UAS-CD8-GFP-expressing flies, a plasma membrane residing protein (Fig. S5A,B). Follicle cell specific Vps13 downregulation did not affect the Vps13-specific signal in the nurse cells (Fig. 4A,B). Conversely, when Vps13 was downregulated in the germ line cells (including the nurse cells), the distinct pattern associated with nurse cell boundaries was lost (Fig. 4C).

Importantly, when Vps13 was downregulated in the follicle cells, no increase in PNCN compared with control ovaries was observed (Fig. 4D). In contrast, knockdown of Vps13 in the germ cells, including the nurse cells, resulted in a significant increase in the percentage of stage-14 egg chambers with PNCN when compared with controls (Fig. 4D). These results indicate that Vps13 is expressed in nurse cells, and downregulation of Vps13 specifically in nurse cells impairs the process of timely removal of nurse cell remnants. To investigate a possible role of Vps13 in nurse cell clearance in other cells, the ubiquitous actin-GAL4 driver in combination with Vps13 RNAi was used. This RNAi approach resulted in an efficient downregulation of Vps13 in fly extracts;

**Fig. 3. Vps13 is expressed during late stages of oogenesis.**
(A,B) Ovaries were dissected, fixed and immunolabelled with an antibody against Vps13. (A) Various stages of egg chambers of wild-type (WT) flies are shown. The boxed areas represent various developmental stages and are enlarged on the right. Box 1 shows an early stage before stage 10. Vps13 signal is present in a pattern reminiscent of nurse cell boundaries (green arrowheads). Box 2 shows an egg chamber at stage 10. Vps13 signal is present in a pattern reminiscent of nurse cell boundaries (green arrowheads). Box 3 shows an egg chamber at stage 11-12. An intense Vps13 signal (green arrowheads) is present, reminiscent of nurse cell boundaries. Nurse cells at this stage are decreasing in size. Box 4 shows a stage-13 egg chamber – the nurse cells are further degraded and the nurse cell compartment is further decreased in size. The Vps13 signal is not visible at this stage. Large red arrows (boxes 3 and 4) indicate nurse cells in advanced stage of degradation. In boxes 1, 3 and 4, a signal is also visible in follicle cells, indicated with small blue arrows. (B) Various stages of egg chambers of Vps13[null] mutants are shown. The boxed areas represent various stages, comparable with the stages in A, and are enlarged. No specific signal is present in mutants. Scale bars: 100 µm.

however, Vps13 expression specifically in nurse cells was not affected (Fig. S6A,B). Under these conditions a PNCN phenotype was also observed (Fig. S6C). This phenotype was partially rescued when human VPS13A was expressed by using the actin-GAL4 driver in the Vps13[PB/PB] mutant background (Vonk et al., 2017; Fig. S6D); however, no human Vps13A expression was observed in ovaries (Fig. S6E). Human VPS13A was observed in fly head extracts under these conditions. These experiments indicate that ubiquitous downregulation of Vps13 in multiple organs and cells can also induce a PNCN phenotype. Previously, a PNCN phenotype was reported in autophagy, cell engulfment, caspase, lysosomal and acyltransferase mutants (Barth et al., 2011; Bass et al., 2009; Baum et al., 2007; Etchegaray et al., 2012; Peterson and McCall, 2013; Wang et al., 2010). In addition, the presence of PNCN is influenced by feeding conditions (Peterson and McCall, 2013). Except for acyltransferase, caspase and engulfment activities, *Drosophila* Vps13 and human VPS13A play a role in all these processes and more (Kumar et al., 2018; Muñoz-Braceras et al., 2019, 2015; Vonk et al., 2017; Yeshaw et al., 2019). Why downregulation of Vps13 in multiple tissues and cells lead to a PNCN phenotype, and which cell types other than nurse cells are involved, is currently not clear. Most likely the reduced fecundity and small ovary-phenotype are also due to a combination of defects caused by the absence of Vps13 in multiple cell types in the mutants. Because downregulation of Vps13 specifically in nurse cells was sufficient to induce a PNCN phenotype and a distinct Vps13 localization pattern was observed in nurse cells, we focused on this cell type.

## Vps13 is associated with the nurse cell plasma membrane and the ER
We further investigated the localization of Vps13 protein in the nurse cells. As mentioned above, Vps13 localizes to the contours of the nurse cell (Fig. 3). However at late stages of oogenesis, the plasma membrane appears very close to the nucleus (Okada and Waddington, 1959). This is because of the large size of the nurse cell nuclei combined with the severely reduced volume of the

cytoplasm owing to cytoplasmic dumping. To determine whether Vps13 is closely associated with the plasma membrane or with the nucleus, we visualized Vps13 and Lamin, a protein associated with the nuclear membrane (Fig. S7, Fig. S8) at stage 11-12. At this stage the Vps13 signal is most intense, nurse cell nuclei show characteristics of dying cells and display typical nuclear invaginations and irregularities (Fig. S7A) (Yalonetskaya et al., 2020). Co-staining of Vps13 and Lamin in wild-type late-stage nurse cells showed that Vps13 does not co-localize with the nuclear cortex (Lamin) but is instead adjacent to it (Fig. S7A-A′, white arrows). It is particularly obvious that Vps13 is not present in nuclear invaginations. It is also important to note the gap between Lamin staining and Vps13 (Fig. S7A′, green asterisk). Taken together, we conclude that Vps13 is not following the contours of the nuclear envelope but rather the contours of the plasma membrane.

To more precisely define the association of Vps13 to the plasma membrane, we expressed the plasma membrane marker mCD8-GFP in nurse cells of a wild-type egg chamber using nanos-GAL4 (Fig. 5A). Co-staining with the Vps13 NT antibody revealed that Vps13 localizes close to the nurse cell plasma membrane but does not completely overlap with it. In fact, Vps13 appears to be localized at the cytoplasmic side of the plasma membrane (Fig. 5A′, red arrowheads). These observations are in line with Vps13 being cytosolic, closely associated to membrane structures and not an integral membrane protein (John Peter et al., 2017; Kumar et al., 2018; Vonk et al., 2017; Yeshaw et al., 2019). Thus, Vps13 is specifically associated with the nurse cell plasma membrane. Yeast Vps13 is involved in trans-Golgi network-related transport and fusion (De et al., 2017) and in mammalian cells VPS13A is associated with the endoplasmic reticulum (ER) (Kumar et al., 2018; Yeshaw et al., 2019) Therefore, we investigated a possible association with *Drosophila* Vps13 and these cell organelles. For these studies we focused on stage-12 egg chambers in which the intense Vps13 signal was visible. Vps13-GFP was detected adjacent to the GM130 Golgi marker (Riedel et al., 2016); however, no
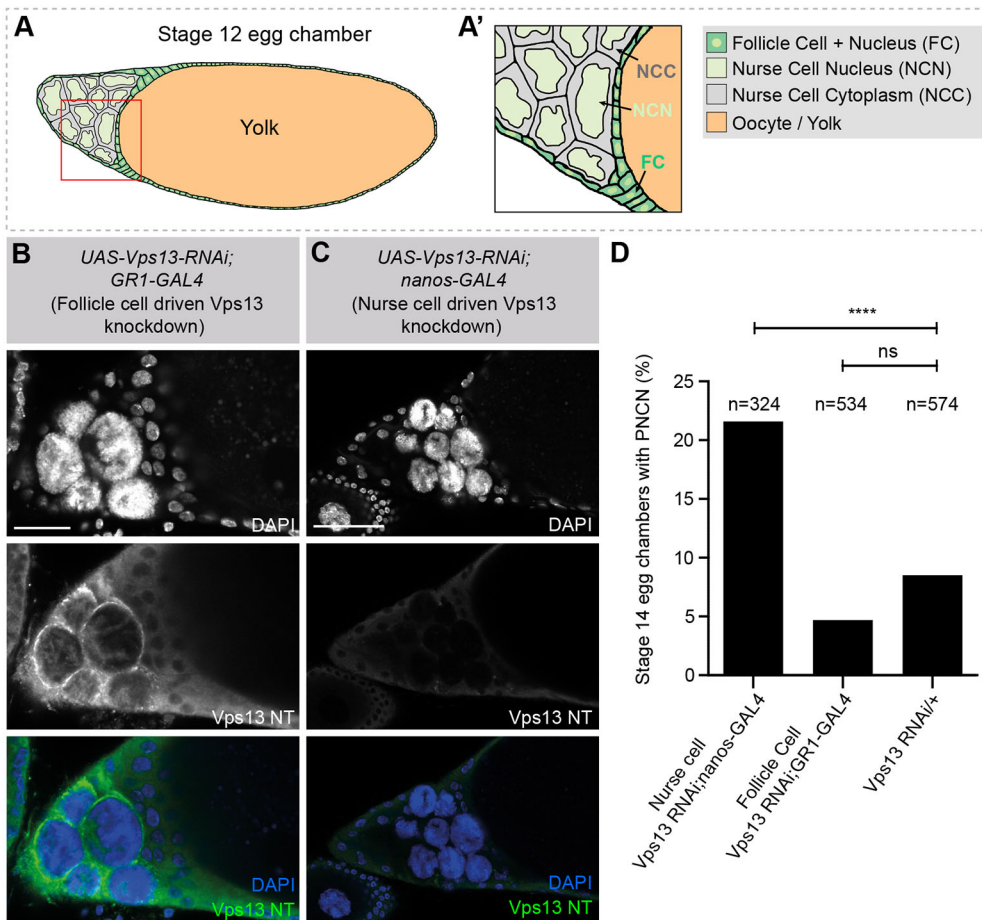
**Fig. 4. Downregulation of Vps13 in nurse cells and not in follicle cells leads to the accumulation of PNCN.**
(A) Schematic representation of a normal stage-12 egg chamber.
(A′) Enlarged view of boxed area in A. (B,C) Stage-12 egg chamber of *Vps13 RNAi/+;GR1-GAL4/+* (targeted Vps13 downregulation in follicle cells) (B) and *Vps13 RNAi/+;nanos-GAL4/+* (targeted Vps13 downregulation in germ line cells including nurse cells) (C), stained with DAPI (blue) and Vps13 NT antibody (green). Scale bars: 50 μm. (D) Quantification of the percentage of stage-14 egg chambers containing PNCN in various genetic backgrounds; *Vps13 RNAi/+;nanos-GAL4/+*, *Vps13 RNAi/+;GR1-GAL4/+* and *Vps13 RNAi/+*(control). ****$P<10^{-6}$ (Fisher's exact test). ns, not significant.

co-localization was observed, and the Vps13-GFP pattern was not similar to the GM130-positive signal (Fig. S9). To investigate a possible co-localization with Vps13 and the ER, the ER marker PDI (Zhu et al., 2003) was used. Upon close inspection, in addition to the intense Vps13 ring-like signal, a faint reticular Vps13-GFP signal was observed (Fig. 5B-C‴). This reticular Vps13 signal was similar and overlapping with the PDI-positive signal (Fig. 5C). The reticular Vps13 and PDI-positive signal was also in close association with the intense membrane-associated Vps13 ring-like signal (Fig. 5C). These data suggest that Vps13 is in close association with the ER, localized in a reticular pattern in the remaining cytoplasm in nurse cells, and enriched at sites where the ER is in close association with the plasma membrane.

**Vps13 acts downstream of programmed cell death during late-stage oogenesis**
Accumulation of persistent nurse cell nuclei can be indicative of a defect in either cell death induction or removal of the dying cells. To assign the cellular process for which Vps13 is required, we examined different aspects of PCD and dead cell removal in the *Vps13* mutants and compared them with wild-type counterparts. Wild-type nurse cells undergoing stage 11-12 PCD display pyknotic nuclei, in which the nuclei show invaginations of the nuclear membrane. In addition, their cytoplasm becomes acidic and this can be visualized by the presence of large LysoTracker-positive structures (Bass et al., 2009; Timmons et al., 2017, 2016). Note that PCD of the individual nurse cells may occur asynchronously even in a single egg chamber (Bass et al., 2009; Timmons et al., 2017, 2016). As in wild type, *Vps13* mutant egg chambers also showed pyknotic nuclei, demonstrated by

small nuclei with intense DAPI staining, which partly remain visible as persistent nuclei (Fig. 2B, green arrows; Fig. S10, red arrowheads). Furthermore, nuclear invaginations, indicative of dying nurse cells (Yalonetskaya et al., 2020), were observed equally well in the wild-type (Figs S7A and S8B) and *Vps13* mutant nuclei (Figs S7B and S10A), strengthening the notion that induced cell death is not impaired in a Vps13-depleted background.

We performed LysoTracker staining and we first analysed stage-13 egg chambers. This analysis revealed that, at stage 13, nurse cell acidification occurred in *Vps13* mutants comparable with that seen in the controls (Fig. 6A,B; Fig. S10). At stage 14, in control egg chambers the number of persistent nurse cell nuclei is low (Fig. 2D), and less than 20% of these persistent nurse cell nuclei are positive for LysoTracker (Fig. S10). In the *Vps13* mutant background the percentage of LysoTracker-positive persistent nurse cell nuclei at stage 14 was 50-80% (Fig. S10). Together, this indicates that in the *Vps13* mutant background acidification initiation is comparable with controls; however, the clearance downstream from the onset of acidification may be delayed. In addition, the Vps13 protein does not co-localize with LysoTracker-positive structures (Fig. 6C,C′). Taken together, we show that all tested characteristics of dying nurse cell processes and the early steps of nurse cell acidification are not impaired in *Vps13* mutants.

**Vps13 localization is independent of the phagocytic receptor Draper and Draper localization is not affected in *Vps13* mutants**
The follicle cell-dependent phagocytic machinery is required for removing dying nurse cells, a process in which the engulfment gene
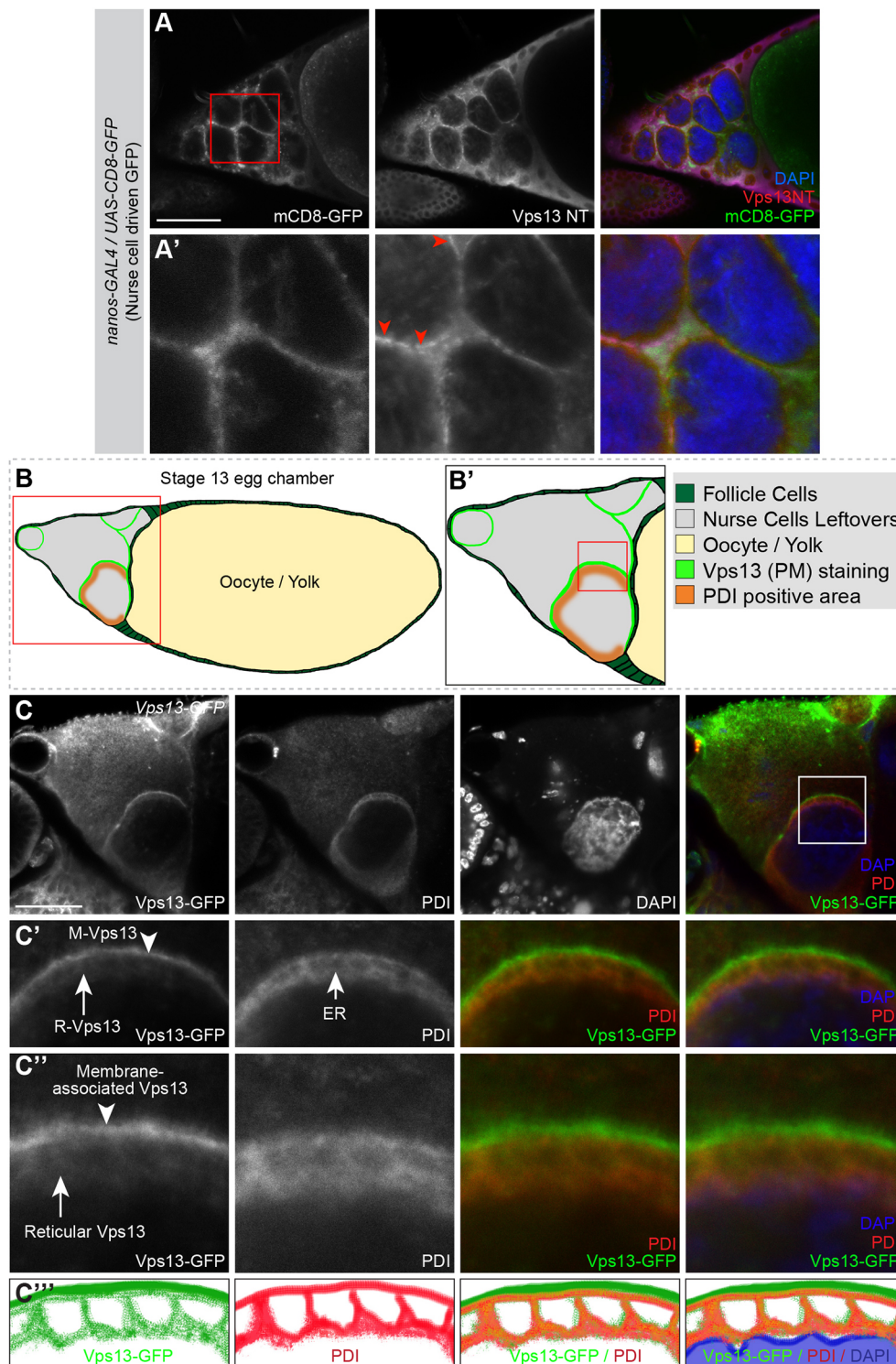
**Fig. 5. Vps13 is closely associated with the plasma membrane and the ER of nurse cells.** (A) Stage-12 egg chambers of wild-type flies with the expression of mCD8-GFP (green in the overlay image) in the nurse cells (*UAS-mCD-GFP; nanos-GAL4:VP16*). Nuclei are visualized by DAPI staining (blue in the overlay image) and the Vps13 NT antibody staining is visualized in red (in the overlay image). (A′) Enlarged view of boxed area in A. Arrowheads indicate the intense signal of Vps13 (red) in close association with the cytoplasmic site of the plasma membrane (green). (B,B′). Schematic showing the stage-12 egg chamber visualized in C. B shows the entire egg chamber, B′ shows an enlarged view of the boxed area in B that is visualized in C. (C-C″) The Vps13-GFP expressing line was used to visualize VPS13, PDI was used as an ER marker, DAPI was used to visualize nuclei. The squares in B′ and C correspond with the enlarged area in C′. In C′ the intense plasma membrane-associated Vps13-GFP signal [Membrane-associated (M-)Vps13; arrowhead] is visible and a less intense reticular Vps13-GFP signal, which is reminiscent to the ER signal [Reticular (R-)Vps13; arrow], is visualized by PDI (ER marker). The area is further enlarged in C″ and schematically visualized in C‴. Scale bars: 50 μm (A,C).

*draper* plays an essential role (Timmons et al., 2017). To test a possible interaction between Draper and Vps13, we stained for Draper in late-stage *Vps13-GFP* ovaries. In line with published results (Etchegaray et al., 2012; Timmons et al., 2016) and its role in follicle cells, a specific Draper signal was detected in follicle cells surrounding and intercalating between the late-stage nurse cells (Fig. 7A,B, Fig. S11B). Draper localization was not affected in the *Vps13* mutants (Fig. 7C,D, Fig. S11A), suggesting that the localization of Draper and the formation of follicle cell protrusions surrounding the nurse cells is

not Vps13 dependent. Conversely, the typical Vps13 localization pattern reminiscent to the boundaries of nurse cells was not changed in the *draper* mutant (*drpr$^{Δ5}$*) compared with the wild type (Fig. 7E,F). Moreover, although in close proximity, no overlap was observed between the Vps13 and Draper signal (Fig. S11C-C″).

These results suggest that Draper and Vps13 do not directly interact and their localization pattern is independent from each other during removal of nurse cell nuclei. Our results do not exclude an indirect interaction of Vps13 and Draper-dependent processes.
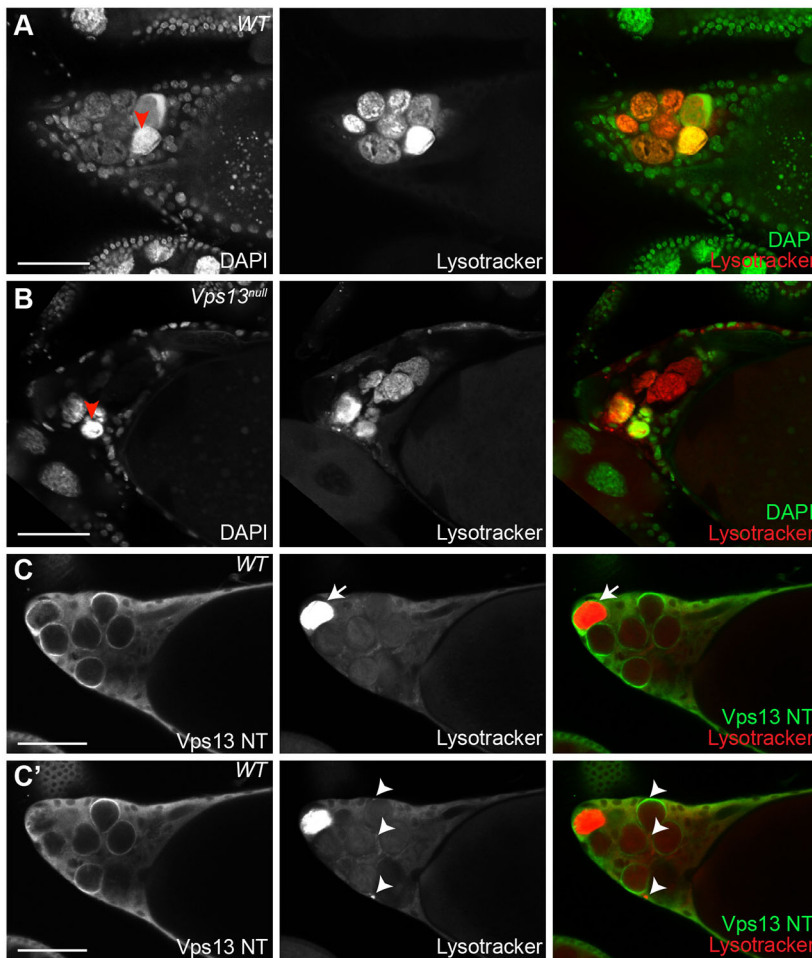
DEVELOPMENT

**Fig. 6. Nurse cell acidification during developmental PCD is not affected in Vps13 mutants.** (A,B) Stage-12 egg chambers of wild-type (WT) controls (A) and *Vps13^null* mutants (B) were labelled with DAPI (green) and LysoTracker (red) to visualize acidification of nurse cell nuclei. Degrading pyknotic nurse nuclei are indicated with red arrowheads. Scale bars: 50 μm. (C,C′) Different optical focal planes of a wild-type stage-12 egg chamber labelled with Vps13 (green) and LysoTracker (red). Arrows indicate an acidified nurse cell nucleus. Acidic compartments, most likely lysosomes, are indicated with white arrowheads. Scale bars: 50 μm.

## Largescale ultrastructural analysis of *Drosophila* ovaries reveals a novel Vps13-dependent membrane structure

To reveal the Vps13-dependent process required for timely removal of nurse cell remnants, we performed an ultrastructural analysis comparing wild-type and *Vps13* mutant ovaries, at the specific stage where the fluorescent signal of Vps13 is the most intense. Ovaries were embedded and processed, and semi-thin sections of stage-12 egg chambers were pre-selected using light microscopy (Fig. 8A-A″) and, subsequently, ultrathin sections were generated, contrasted and analysed by large-scale electron microscopy, or nanotomy (Hoffmann et al., 2016; Kuipers et al., 2015; Sokol et al., 2015). This technique allows zooming in and out in a large specimen area, enabling the visualization of the whole egg chamber as well as detailed examination at a very high magnification of every desired area within the specimen (Fig. 8). This technique enables an unbiased approach and full open access to the complete ultrastructural section and presented data. These images are available at www.nanotomy.org.

In control nurse cells, and consistent with our immunofluorescence and previously published data (Nezis et al., 2000) the nucleus (blue) is irregular and pyknotic, the nuclear membrane (dark blue line) is still intact and shows invaginations, the cytoplasmic part of the nurse cells (light magenta) is reduced, the plasma membrane (dark magenta line) is in close proximity to the nuclear envelope, and large translucent vacuoles (yellow) are present (Fig. 8). A degradative process is clearly ongoing, characterized by structures containing cellular degradation products

(orange) and the to-be-degraded nurse cells are surrounded by the engulfing follicle cells (green) (Fig. 8). All of these ultrastructural features are also present in *Vps13* mutant ovaries of the same stage (Fig. 9; Fig. S12), further confirming that the PCD process and the engulfment by follicle cells were not affected in *Vps13* mutants.

The zoom-in options of a relatively large ultrastructural surface allow detailed inspection of the cytosolic part in close proximity to the plasma membrane of the entire nurse cells, where the Vps13 signal was most intense. We noticed one striking difference between wild-type and *Vps13* mutant nurse cells: A thin elongated structure very close to the plasma membrane (green line) was present in nurse cells in wild-type stage 11-12 egg chambers (Fig. 8B″-C″, green arrowheads; Fig. S13). The localization of this ultrastructure is consistent with the Vps13-positive signal as visualized by Vps13 antibody staining and Vps13-GFP expression lines. This structure was nearly absent in all analysed degrading nurse cells present in *Vps13* mutant egg chambers of a comparable stage (Fig. 9; Figs S12, S13). This structure was stained by osmium tetroxide and is therefore likely to be membranous; it appears as a discontinuous double-membrane structure. Close inspection of this structure reveals the presence of structures reminiscent to ribosomes, suggesting that this structure is ER-derived (Fig. S14).

## DISCUSSION

Here, we report a novel role for *Drosophila* Vps13 in the timely removal of dying nurse cells downstream of induced cell death during development. Loss of Vps13 results in the absence of a
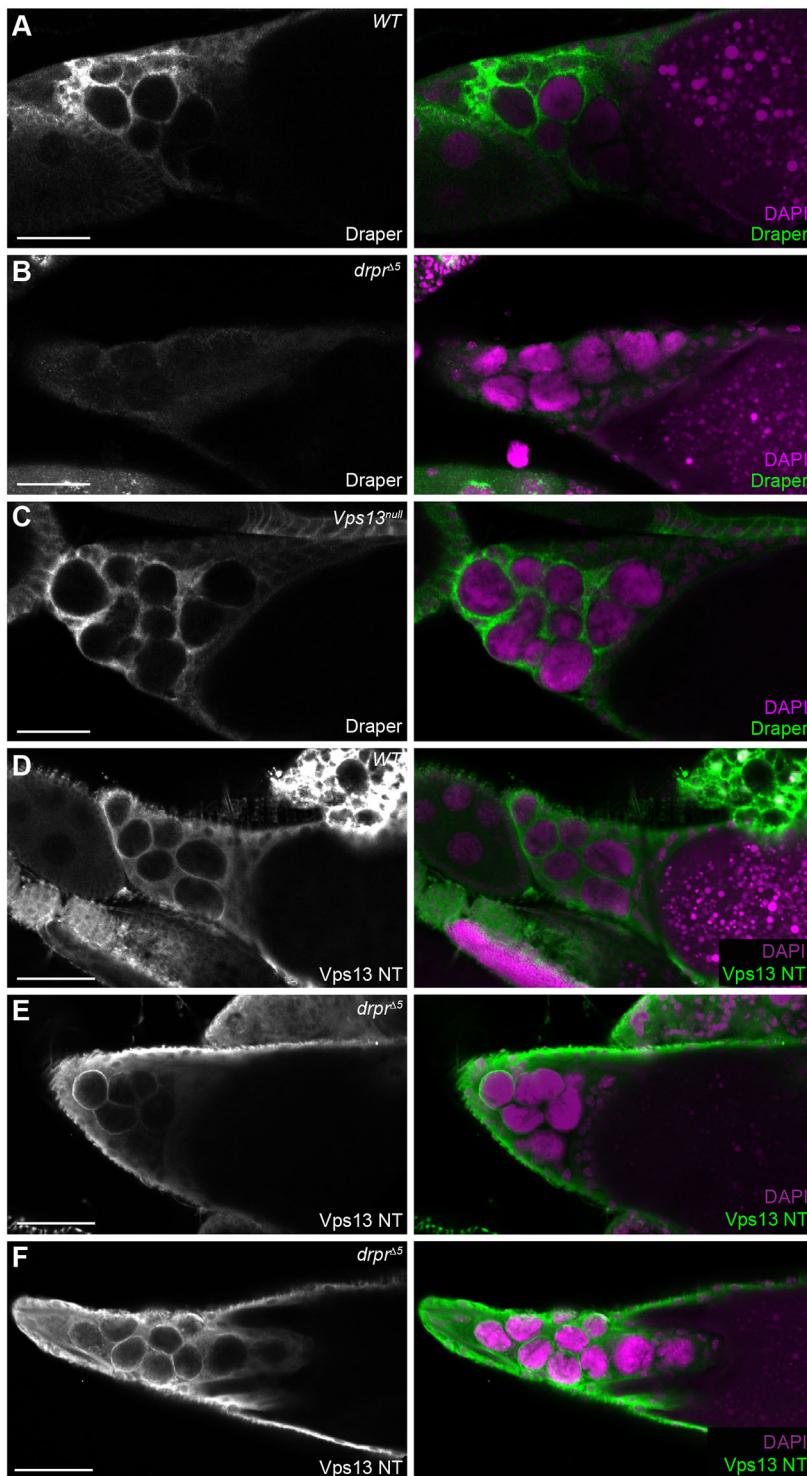
**Fig. 7. Absence of Vps13 does not affect Draper intensity and localization and absence of Draper does not affect Vps13 intensity and localization.** (A-C) Immunolabelling of stage-12 egg chambers with a Draper-specific antibody (green) in wild-type (WT) (A), Drpr^Δ5 mutant (B) and Vps13^null (C) to visualize Draper in ovaries. DAPI (magenta) was used to visualize nuclei. (D-F) Stage-12 egg chambers visualizing Vps13 with Vps13 NT antibody in a wild-type background (D) or in a *draper* mutant background (E,F). Scale bars: 50 μm.

specific membrane structure closely associated with the plasma membrane of dying nurse cells. The immunofluorescence data suggest that this newly identified Vps13-dependent membrane structure is most likely Vps13-rich.

**Nanotomy**

For our electron microscopy (EM) analysis we used nanotomy, a technique for ultrastructural investigations especially suitable when complex tissues are under investigation and when abnormalities within mutants or affected tissues are searched for (Kuipers et al.,

2016). *Drosophila* oogenesis, especially at later stages, is complex to investigate as multiple processes are at stake to ensure nurse cell death and removal. With classical EM techniques, only tiny fragments of the tissue section can individually be analyzed and presented and a Vps13-dependent structure as we present here (Fig. 8C″) could have easily been missed. Our technique enables the visualization of the structure localized over the whole circumference of the plasma membrane of the complete nurse cell, and allows open access of the presented zoomable data for other researchers (www.nanotomy.org).

DEVELOPMENT
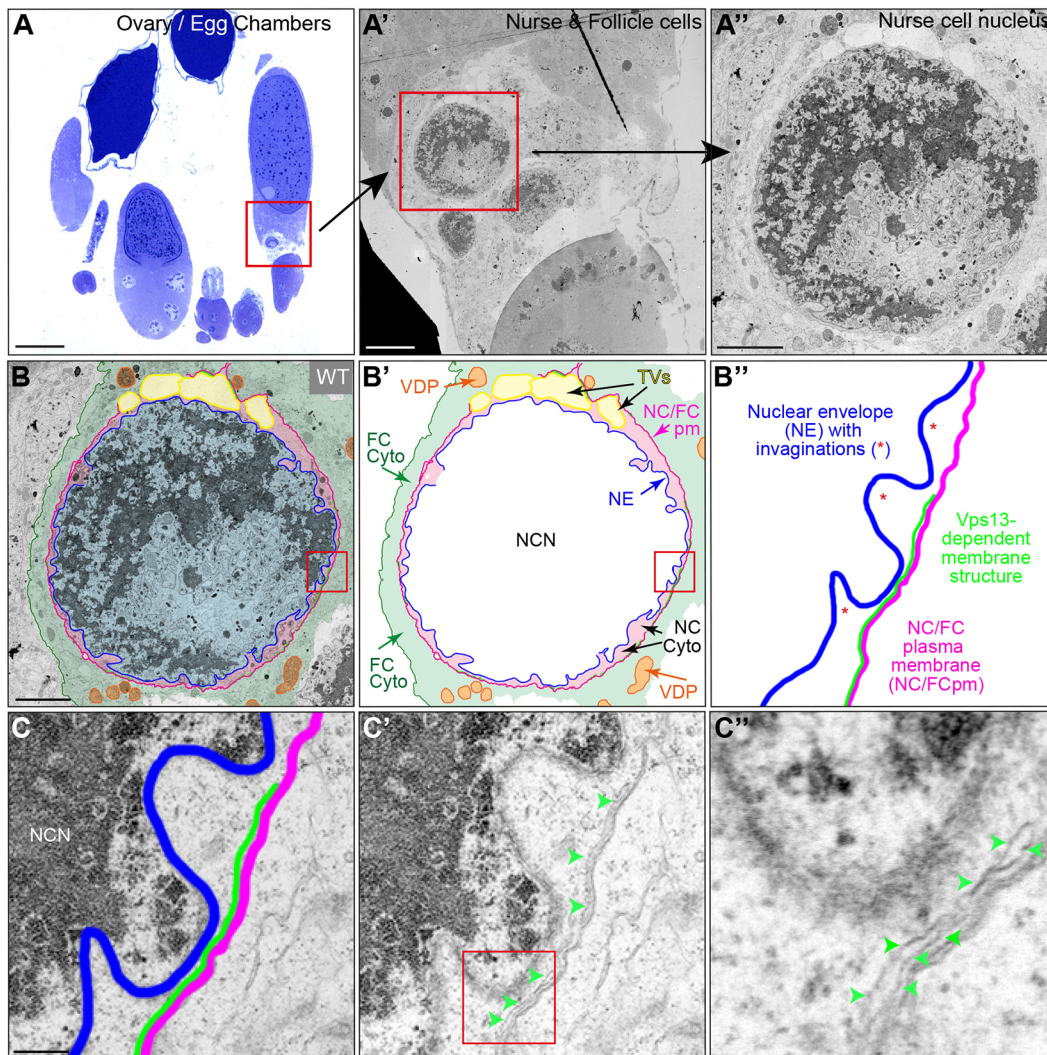
**Fig. 8. Vps13-dependent membrane structure is closely associated with the plasma membrane of nurse cells.** (A) Bright-field microscopic image of a semi-thin section of a wild-type (WT) ovary stained with Toluidine Blue which was used to select the right stage of the egg chamber, after which ultra-thin sections were processed for EM. (A′) Ultra-thin section containing part of the egg chamber harbouring nurse cells of the selected stage. (A″) Enlarged view of boxed area in A′. Access to this section allowing the ability to zoom in is provided via www.nanotomy.org. (B) Large-scale electron microscopic image of the selected egg chamber and region, represented by the boxed area in A and A′, containing nurse cells and follicle cells. Artificial colours were used to indicate engulfing follicle cells (green), nurse cell cytoplasm (magenta), nurse cell nucleus (blue), translucent vacuoles (yellow) and vesicles representative for the degradative machinery (orange). (B′) Schematic containing structures visible in A″ and B. The magenta line indicates the sites of close contact between the plasma membrane of the nurse cell and the plasma membrane of the follicle cell (NC/FCpm), the blue line indicates the nuclear envelope (NE). FC Cyto, cytoplasm of stretch follicle cells; NC Cyto, cytoplasm of nurse cells; TVs, translucent vacuoles; VDP, vesicles containing cellular degradation products. (B″) Schematic of enlarged image of the boxed area in B and B′ showing magnification of a part of the plasma membrane of the nurse cell; the area where the VPS13-dependent structure is present is indicated in light green. (C,C′) Increased magnification of the area presented in B″ with (C) and without (C′) the artificial colours. (C″) Enlargement of the boxed area in C′. Green arrowheads indicate the VPS13-dependent membranous structure localized in close association with the plasma membrane. Scale bars: 200 µm in A; 20 µm in A′; 5 µm in A″,B; 500 nm in C.

## A possible lipid exchange role for Vps13 at membrane contact sites

In various organisms it has been demonstrated that products of the VPS13 gene family are localized at the interphase of membranes of various organelles. In yeast, Vps13 is present at contact sites between the mitochondria and the vacuole and between the vacuole and the ER (Lang et al., 2015). In mammalian cells VPS13A is closely associated at ER-mitochondria contacts (Kumar et al., 2018; Muñoz-Braceras et al., 2019; Yeshaw et al., 2019) and VPS13C is at contacts between the ER and late endosomes/lysosomes (Kumar et al., 2018). In VPS13A-depleted cells, ER-mitochondria contact sites are decreased (Yeshaw et al., 2019) and in cells overexpressing VPS13A, ER-mitochondria contact sites are increased (Kumar

et al., 2018). In addition, the N-terminal structure of VPS13 harbours characteristics of having a lipid transporting function (Kumar et al., 2018; Li et al., 2020). A preference of phosphatidylcholine was observed based on the identification of lipid species co-purified with the N-terminal part of VPS13 (Kumar et al., 2018). Together, this indicates that VPS13 enables associations between membranes of various organelles and thereby enables the transfer of glycerophospholipids and possible other lipid species between membranes of the tethered organelles. Our observation of a Vps13-dependent membrane structure close to the plasma membrane is consistent with these findings. Based on the co-localization studies of Vps13 and the ER (Fig. 5C) and the ultrastructure of this membrane entity (which also sometimes
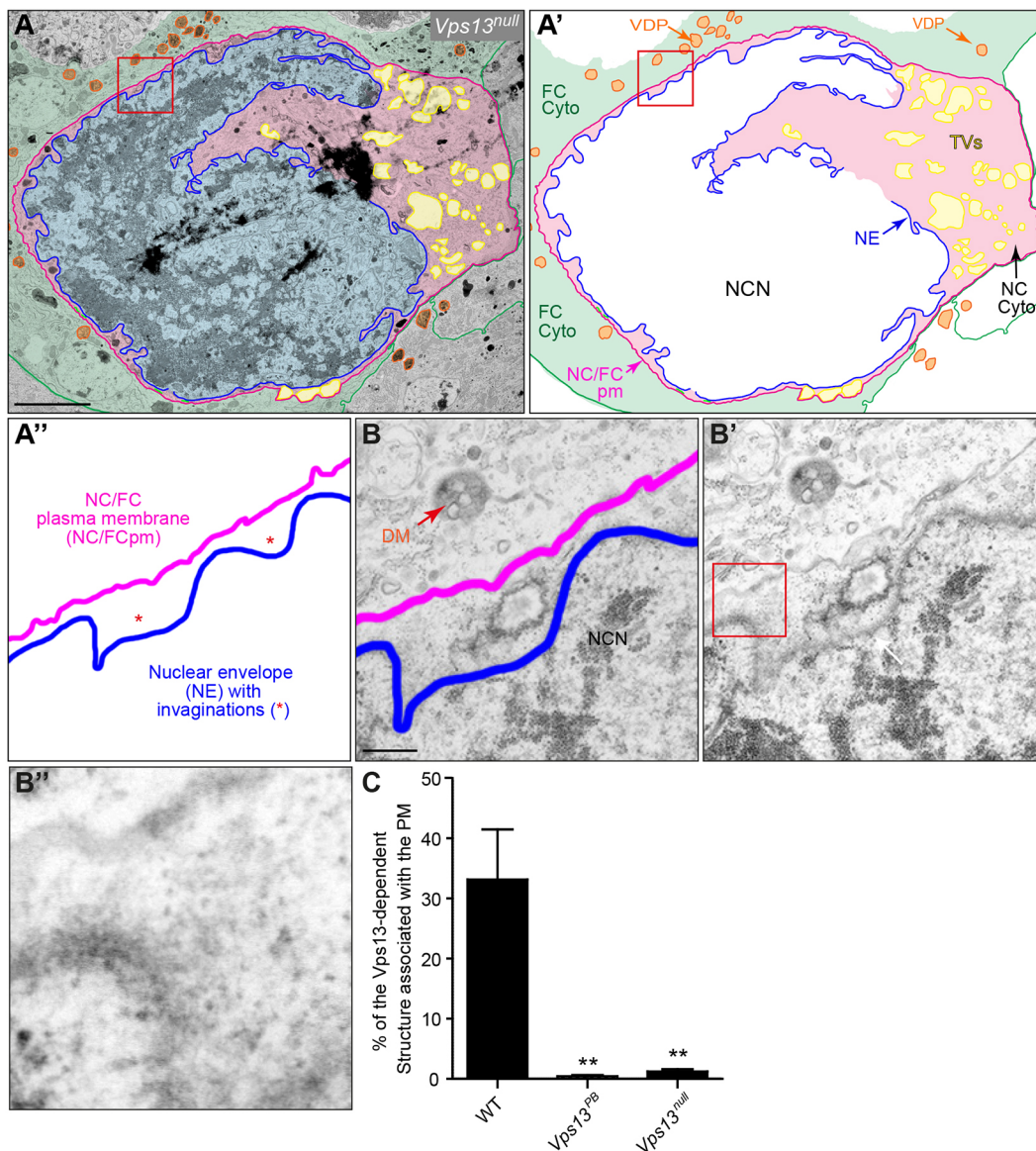
**Fig. 9. Membrane structure is absent in *Vps13* mutants.** (A-B″) Ultrastructural analysis (as in Fig. 8) of egg chambers of the *Vps13^null^* mutant. (A) Large-scale EM image of the selected region, containing nurse cells and follicle cells (www.nanotomy.org). (A′) Schematic containing structures visible in A. (B,B′) Increased magnification of the area presented in A″ with (B) and without (B′) the artificial colours. (B″) Enlarged view of the boxed area in A′. For abbreviations see Fig. 8. Scale bar: 5 µm in A; 500 nm in B/B′. (C) Quantification of the presence of the Vps13-dependent structure. The percentage of the length of the plasma membrane, visible in the sections, which is in close association with a visible membrane structure, as indicated in C-C″, is given for wild type (WT; $n=3$), *Vps13^PB^* ($n=3$) and *Vps13^null^* ($n=3$) mutants. **$P<0.01$ (two-tailed unpaired Student's $t$-test).

contains ribosomes; Fig. S14) it may be an ER-derived structure. Our data suggests that Vps13 creates contact sites between the plasma membrane and the ER. It may be possible that owing to the contact sites the Vps13-dependent membrane structure is stabilized and visible. Based on its lipid transport characteristics, it is also likely that lipids are being transferred from the membrane structure to the plasma membrane or vice versa. The Vps13-dependent membrane structure is present around stage 11-13. It may be that at this stage a certain lipid content of the plasma membrane or the Vps13-dependent membrane structure is required to enable an optimal degradation/clearance process. At later stages numerous membrane structures are observed in the to-be-degraded nurse cell corpses. Pieces of chromatin are surrounded by membrane structures and numerous multi vesicular bodies and lysosomes are observed (Fig. S15). It is possible that the plasma membrane of the

nurse cells or the Vps13-dependent membrane structure are a source or play a role in the formation of the numerous membranous structures required for the more downstream degradation process. It may be possible that the lipid composition of the degradation membranes in the absence of Vps13 are not optimal and therefore the degradation process is delayed or less efficient. Mechanisms and characteristics of the degradation processes downstream from the non-apoptotic cell death and the acidification process are currently largely unknown. Here, we identified Vps13 as one cell-autonomous player of these processes. With this knowledge, and the generated tools, it is possible to start from here to unravel processes required for clearance of remnants downstream of non-apoptotic cell death.

Compared with the PNCN phenotype in *draper* mutants, the phenotype in *Vps13* mutants can be classified as mild. It may be

possible that not all nurse cell nuclei are degraded by the same mechanism, and Vps13 only plays a role in degradation of a subset of nurse cells. It is known that nurse cell degradation is asynchronous and some nurse cell nuclei are degraded later than others (Mondragon et al., 2019). Therefore, an alternative explanation is that nurse cell degradation is less efficient in the *Vps13* mutants and this only leads to the persistence of those nurse cell nuclei that are degraded relatively late.

## ChAc may be caused by impairment in the timely removal of dead cell corpses

Less efficient clearance of death cell corpses may be an underlying theme in phenotypes associated with ChAc, the human disease associated with VPS13A mutations. In ChAc patients two distinct characteristics are observed: neurodegeneration and acanthocytosis. A possible explanation for these two seemingly independent phenotypes is currently missing. Interestingly, efficient clearance of cell corpses is required both for healthy brain function as well as for timely removal of aging erythrocytes (Poon et al., 2014). Consistent with our observations in *Drosophila* ovaries, it may therefore be that both characteristics of the disease can be explained by less efficient clearance of to-be-degraded cells in the circulation and in the brain.

In summary, we demonstrate the localization and a novel function for Vps13 in a relatively large cell type in an essential developmental process. Our work will be of interest in various fields ranging from understanding the function of Vps13 proteins in membrane contact sites, their roles in human diseases and to understand mechanisms of factors playing a role in clearance of cell debris downstream from non-apoptotic induced cell death.

## MATERIALS AND METHODS
### *Drosophila* maintenance
*D. melanogaster* stocks and crosses were raised on the standard cornmeal used at the Bloomington *Drosophila* Stock Center (BDSC; Nutri-Fly Bloomington Formulation, 66-113) at 25°C. For lifespan experiments standard agar food was used. The following stocks were collected from the BDSC: *w1118* (in the text referred to as wild type); *actin-GAL4/TM6B* (3954); *actin-GAL4/CyO* (4414); *nos-GAL4:VP16* (64277, here called nanos-GAL4); *UAS-mCD8-GFP* (5137); *Vps13 RNAi* (38270). The *Vps13^PB^* mutant (*Vps13^c03628^*), precise excision line (Excision line 1) and *UAS-hVps13A* line are described in and obtained from Vonk et al. (2017). The *GR1-GAL4* line was a generous gift from Trudi Schüpbach (Princeton University, Princeton, USA). The *w;Sp/CyO;DrprΔ5rec9/TM6b* line, here referred to as *drprΔ5*, was a generous gift from Mark Freeman (Vollum Institute, Portland, USA).

### *Drosophila* female fecundity assay
To investigate female fecundity and egg lay, 10 freshly eclosed females were housed on apple juice agar plates supplemented with yeast paste. Three *w1118* males were included to ensure mating. Flies were transferred to fresh plates every 24 h and the number of eggs laid in each 24 h period was recorded for 14 days. For Fig. 1C,D for all indicated fly lines, cages of ~100 cm³ were used; for Fig. S1B for all fly lines, cages of ~50 cm³ were used.

### *Drosophila* life span
One-day-old male adult CRISPR/Cas9-treated flies were collected with the appropriate control and kept on standard agar food at 25°C. Flies were housed in fly food vials with 10-20 flies each and put into fresh vials every 2 or 3 days. The incidence of dead flies was counted every 2 or 3 days.

### Generation of a *Drosophila Vps13^null^* mutant and *Vps13-GFP* line using the CRISPR/Cas9 system
We used the CRISPR/Cas9 system to generate a *Vps13* null mutant. In addition, we constructed a fly line expressing a Vps13-GFP fusion protein. For the generation of the *Vps13* null mutant we designed two sgRNAs

targeting either exon 4 or exon 8 of the *Vps13* gene (Table S1). For selection of the sgRNA the DRSC Find CRISPR Tool was used (https://www.flyrnai. org/crispr/). Each of the sgRNAs was cloned into the pU6-BbsI-chirRNA plasmid (Addgene plasmid #45946; gift from Melissa Harrison, Kate O'Connor-Giles and Jill Wildonger, University of Wisconsin-Madison, USA) via BbsI restriction sites (Gratz et al., 2013). Both constructs were injected simultaneously into transgenic embryos expressing Cas9 in the germline [yw;;nos-Cas9(III-attP2)/TM6C] by BestGene. Potential mutant lines were balanced with a *CyO* second chromosome balancer. Because homozygous males of the original Vps13PB stock are sterile, offspring homozygous for the potential mutant Vps13 allele were screened for male sterility and used for further studies. Fly lines that were male sterile were analyzed on western blot with antibodies directed to the N-terminal and C-terminal part of the Vps13 protein (Vonk et al., 2017) to identify new *Vps13* null mutants.

For the creation of the *Vps13-GFP* line, one sgRNA was designed directed against the 3′ end of the *Vps13* gene and cloned into the pU6-BbsI-chirRNA vector (for primers, see Table S1). A HDR plasmid was created in pBluescript II SK+ (Stratagene) with Gibson assembly Cloning kit (New England Biolabs). Briefly a 5′ and 3′ flanking arm of about 1.2 kbp and eGFP were created with PCR, all three products were inserted in pBluescript II SK+ that was linearized with NotI and EcoRV (for primers, see Table S2). Injection of the sgRNA and HDR plasmid and further balancing of potential *Vps13-GFP* lines was carried out as described before. Potential *Vps13-GFP* lines were screened for the presence of GFP using PCR. *Vps13^null^* and *Vps13-GFP* lines were confirmed by sequencing.

### RNA isolation and quantitative real-time PCR of CRISPR/Cas9-treated flies
Flies of *Vps13^null^* and CC Control were collected and snap frozen in liquid nitrogen. The samples were lysed in TRIZOL (Invitrogen) for RNA extraction and reverse transcribed using M-MLV (Invitrogen) and random primers (Invitrogen). Relative changes in transcript levels were determined on the CFX Connect (Bio-Rad) using SYBR green supermix (Bio-Rad). Calculations were carried out using the relative CT method. For each primer set the PCR efficiency was determined. The sequences of primers used are listed in Table S3. The expression levels were normalized for *rp49* (housekeeping gene; also known as *RpL32*). Primer set 1 was directed to the N-terminus of *Vps13* upstream of the gRNA. Primer set 2 was directed to a sequence downstream of the PiggyBac insertion site of the *Vps13^c03628^* mutant.

### Genomic DNA isolation and PCR screening of potential *Vps13-GFP* flies
To isolate *Drosophila* genomic DNA (gDNA) from the potential *Vps13-GFP* flies, two different protocols were used: (1) Two flies of the potential *Vps13-GFP* lines were collected and mashed for 20-30 s in 100 μl squishing buffer [10 mM Tris-HCl (pH 8.2), 1 mM EDTA, 25 mM NaCl and 400 μg/ml proteinase K]. After 30 min incubation at 37°C the proteinase K was inactivated by heating the samples to 95°C for 3 min. The samples were centrifuged shortly at 1000 *g* and the supernatant was used for PCR. (2) Five flies of the potential *Vps13-GFP* lines were collected and mashed for 20-30 s using a yellow pipet tip with 50 μl solution A [0.1 M Tris-HCl (pH 9.0), 0.1 M EDTA and 1% SDS]. Then samples were incubated at 70°C for 30 min. Afterwards 7 μl 8 M KAc (Merck) was added per sample and samples were incubated on ice for 30 min. The samples were centrifuged for 15 min at 13,000 rpm (17,949 *g*) at 4°C after which the supernatant was transferred to a fresh tube. Then 30 μl of isopropanol (Sigma-Aldrich) was added to each sample and after some shaking the samples were centrifuged for 5 min at 10,000 rpm (10,621 *g*) at 4°C. Afterwards the supernatant was removed and the pellet was washed with 70% EtOH and centrifuged for 5 min at 13,000 rpm (17,949 *g*). After removing the supernatant, the pellet was air-dried and the pellet was resuspended in 20 μl RNAse- and DNAse-free H₂O (Life Technologies).

The DNA sequences of the potential *Vps13-GFP* lines were initially screened for presence of *GFP* (gDNA isolation method 1) using the 'GFP' primers listed in Table S4. A small selection of lines positive for GFP were then further analyzed by PCR for the flanking regions of the *GFP* sequence to check whether the *GFP* was fused to the 3′ of the *Vps13* gene (gDNA

isolation protocol 2) using the 'GFP+flanking regions' primers listed in Table S4. DNA sequences were amplified using Paq5000 Hotstart PCR Master Mix (Agilent), run on a 0.8% agarose gel and visualized with the Chemidoc MP System (Bio-Rad).

### Drosophila ovary dissection
*Drosophila* female flies were collected 0-8 h after eclosion and kept on standard BDSC food supplemented with yeast paste at 25°C. Three to five control (*w1118)* males were added to ensure mating and to stimulate oogenesis. Ovaries of 4-day-old females were dissected in PBS and imaged immediately using a Leica M165 FC microscope for size analysis or fixed in 4% formaldehyde (Thermo Fisher Scientific) in PBS for further antibody staining.

### Antibody staining and microscopy
Ovaries of 4-day-old females were dissected in PBS and fixed for 30 min in 4% formaldehyde in PBS at room temperature (RT). The fixed tissue was washed three times for 10 min in PBS+0.1% Triton X-100 (Sigma-Aldrich) and afterwards permeabilized with PBS+0.3% Triton X-100 for 1 h followed by an optional blocking step with PBS+5% bovine serum albumin for 1 h. The following antibodies were used: rabbit anti-Vps13 NT (1:500, Vonk et al., 2017), mouse anti-Draper 5D14 [1:100, Developmental Studies Hybridoma Bank (DSHB)], mouse anti-Lamin (1:400, DSHB), rabbit anti-GM130 (1:200, Abcam, ab52649), mouse anti-PDI (1:200, Enzo Lifesciences, 1D3). Appropriate secondary antibodies used were: Alexa 488- or Alexa 594-conjugated antibodies [Invitrogen A-11001 (goat anti-mouse), A11005 (goat anti-mouse), A-11008 (goat anti-rabbit) and A-11012 (goat anti-rabbit)] used at 1:500. Nuclear staining with 4′,6-diamidino-2-phenylindole (DAPI; 0.2 µg/ml) was performed together with the secondary antibody staining. LysoTracker Red DND-99 (20 µM, Invitrogen) was used to detect acidification of nurse cells. Freshly dissected ovaries were incubated with LysoTracker for 3 min at RT. After a short wash with PBS, ovaries were fixed according to standard protocol described above and stained with DAPI. Ovaries were mounted in CitiFluor (Agar Scientific) or 80% glycerol and analyzed on a Zeiss-LSM780 NLO confocal microscope using Zeiss Zen software. Adobe Photoshop and Illustrator were used for image assembly.

### Ovary sample EM processing
Ovaries of 4-day-old female flies were dissected and fixed overnight on a rotator at 4°C in freshly prepared fixative containing 2.5% glutaraldehyde in 0.1 M sodium cacodylate buffer (pH 7.4). Samples were processed as previously described (Sokol et al., 2015). In brief, after three short washes with 0.1 M sodium cacodylate buffer samples were post-fixed using 1% osmium tetroxide and 1.5% potassium ferrocyanide in 0.1 M sodium cacodylate buffer for 2 h at 4°C. Then samples were washed with milliQ water at RT followed by dehydration in an ethanol series. Finally the samples were embedded in epoxy-resin (epon). Semi-thin sections (500 nm) were stained with Toluidine Blue dye and used to select the correct stage of egg chambers after which ultra-thin sections (70 nm) were collected on formvar-coated single slot copper grids and contrasted with 2% uranyl acetate in water for 20 min followed by Reynolds lead citrate for 2 min. Images were acquired on a Supra 55 scanning EM (SEM; Zeiss) using a scanning transmission EM (STEM) detector at 2.5 nm pixel size using an external scan generator with ATLAS 5 (Fibics) software as described by Kuipers et al. (2016). Individual tiles were stitched and data was exported as an html file or were converted to czi files and areas of interest were selected and exported as BIG-TIF images using Zeiss Zen software for further image analysis in Adobe Photoshop.

### Western blot analysis
For samples of fly heads, flies were snap frozen in liquid nitrogen and decapitated using a vortex. Then 4 µl of 2× Laemmli buffer [2% SDS, 10% glycerol, 0.004% bromophenol blue, 0.0625 M Tris-HCl (pH 6.8)] containing 0.8 M urea and 50 mM DTT was added per fly head. For samples of ovaries, 4-day-old females were dissected in PBS and ovaries were snap frozen in liquid nitrogen. Per ovary, 4 µl of 2× Laemmli buffer with 0.8 M urea and 50 mM DTT was added. Samples were sonicated five times for 5 s and boiled for 5 min. Protein extracts were run on 8% polyacrylamide gels, transferred onto PVDF membranes overnight using transfer buffer containing 10% methanol. Membranes were blocked with 5%

milk in PBS 0.1% Tween-20 and subsequently incubated with primary antibodies overnight at 4°C. The primary antibodies used were: rabbit anti-Vps13 #62 (1:1000, Vonk et al., 2017), anti-Vps13 NT (1:1000, Vonk et al., 2017), mouse anti-GFP (1:5000, Clontech, 632381), mouse anti-α-tubulin (1:5000, Sigma-Aldrich, T5168), rabbit anti-human VPS13A (1:1000, Sigma-Aldrich, HPA021662). Appropriate secondary HRP-conjugated antibody staining [1:5000, GE Healthcare, GENA934 (anti-rabbit) or GENXA931 (anti-mouse)] was carried out at RT in 5% milk for both Vps13 antibodies and PBS 0.1% Tween-20 for GFP and α-tubulin. Detection was performed using ECL or super-ECL solution (Thermo Fisher Scientific) with the ChemiDoc Touch (Bio-Rad). Figs S16-S18 show full scans of all blots.

### Quantifications and statistical analysis
To quantify the percentage of PNCN, ovaries stained with DAPI were analyzed using a Leica fluorescent microscope. Quantification was performed by calculating stage-14 egg chambers with PNCN divided by all stage-14 egg chambers analyzed and presented as a percentage.

Data were analyzed using GraphPad Prism5 statistical software. Statistical significance was determined using Student's *t*-tests or Fisher's exact test, as stated in the legends. Data are represented as mean±s.e.m. unless otherwise indicated. $P$-values below 0.01 were considered significant. In the figures **$P<0.01$, ***$P<0.001$ and ****$P<10^{-6}$.

For quantification of the Vps13-dependent structure at the ultrastructural level, for each genotype (wildtype, $Vps13^{PB}$ and $Vps13^{null}$) three nurse cells were selected in stage 11-12 egg chambers, in which the nuclear envelope was intact and showed invaginations, the DNA was condensed, the cytoplasm compartment was decreased and the plasma membrane largely intact. The length of visible plasma membrane and Vps13-dependent structures was traced and afterwards measured using Adobe Illustrator and plotted as the percentage of the plasma membrane that was associated with the Vps13-dependent structure using GraphPad Prism. For statistical analysis student's *t*-test was used. Error bars represent mean±s.e.m. ($n$=3). To exclude variability in ultrastructures due to variability in fixation, dehydration, epon embedding and post fixation stainings, samples derived from all genotypes and used for the quantification in Fig. 9B were all generated simultaneously using identical and shared reagents for all preparation steps. The $n$=3 nuclei of each condition were obtained from one epon mounting block per genotype. Additional samples derived from additional epon mounting blocks were obtained for wild-type and Vps13$^{null}$ ovaries (Fig. S13) and consistent results were obtained.

DEVELOPMENT

**Supplementary information**
Supplementary information available online at
https://dev.biologists.org/lookup/doi/10.1242/dev.191759.supplemental

**References**
Barth, J. M. I., Szabad, J., Hafen, E. and Köhler, K. (2011). Autophagy in Drosophila ovaries is induced by starvation and is required for oogenesis. *Cell Death Differ.* 18, 915-924. doi:10.1038/cdd.2010.157
Bass, B. P., Tanner, E. A., Mateos San Martín, D., Blute, T., Kinser, R. D., Dolph, P. J. and McCall, K. (2009). Cell-autonomous requirement for DNaseII in nonapoptotic cell death. *Cell Death Differ.* 16, 1362-1371. doi:10.1038/cdd.2009.79
Bassett, A. R. and Liu, J.-L. (2014). CRISPR/Cas9 and genome editing in Drosophila. *J. Genet. Genomics* 41, 7-19. doi:10.1016/j.jgg.2013.12.004
Baum, J. S., Arama, E., Steller, H. and McCall, K. (2007). The Drosophila caspases Strica and Dronc function redundantly in programmed cell death during oogenesis. *Cell Death Differ.* 14, 1508-1517. doi:10.1038/sj.cdd.4402155
Bean, B. D. M., Dziurdzik, S. K., Kolehmainen, K. L., Fowler, C. M. S., Kwong, W. K., Grad, L. I., Davey, M., Schluter, C. and Conibear, E. (2018). Competitive organelle-specific adaptors recruit Vps13 to membrane contact sites. *J. Cell Biol.* 217, 3593-3607. doi:10.1083/jcb.201804111
Brown, G. C. and Neher, J. J. (2012). Eaten alive! Cell death by primary phagocytosis: 'phagoptosis'. *Trends Biochem. Sci.* 37, 325-332. doi:10.1016/j.tibs.2012.05.002
Brown, G. C. and Neher, J. J. (2014). Microglial phagocytosis of live neurons. *Nat. Rev. Neurosci.* 15, 209-216. doi:10.1038/nrn3710
Chen, Q., Kang, J. and Fu, C. (2018). The independence of and associations among apoptosis, autophagy, and necrosis. *Signal Transduct. Target. Ther.* 3, 18. doi:10.1038/s41392-018-0018-5
Danek, A. and Walker, R. H. (2005). Neuroacanthocytosis. *Curr. Opin. Neurol.* 18, 386-392. doi:10.1097/01.wco.0000173464.01888.e9
De, M., Oleskie, A. N., Ayyash, M., Dutta, S., Mancour, L., Abazeed, M. E., Brace, E. J., Skiniotis, G. and Fuller, R. S. (2017). The Vps13p–Cdc31p complex is directly required for TGN late endosome transport and TGN homotypic fusion. *J. Cell Biol.* 216, 425-439. doi:10.1083/jcb.201606078
Dominguez, A. A., Lim, W. A. and Qi, L. S. (2016). Beyond editing: repurposing CRISPR-Cas9 for precision genome regulation and interrogation. *Nat. Rev. Mol. Cell Biol.* 17, 5-15. doi:10.1038/nrm.2015.2
Etchegaray, J. I., Timmons, A. K., Klein, A. P., Pritchett, T. L., Welch, E., Meehan, T. L., Li, C. and McCall, K. (2012). Draper acts through the JNK pathway to control synchronous engulfment of dying germline cells by follicular epithelial cells. *Development* 139, 4029-4039. doi:10.1242/dev.082776
Foley, K. and Cooley, L. (1998). Apoptosis in late stage Drosophila nurse cells does not require genes within the H99 deficiency. *Development* 125, 1075-1082.
Giorgi, F. and Deri, P. (1976). Cell death in ovarian chambers of Drosophila melanogaster. *J. Embryol. Exp. Morphol.* 35, 521-533.
Gratz, S. J., Wildonger, J., Harrison, M. M. and O'Connor-Giles, K. M. (2013). CRISPR/Cas9-mediated genome engineering and the promise of designer flies on demand. *Fly (Austin)* 7, 249-255. doi:10.4161/fly.26566
Gudipaty, S. A., Conner, C. M., Rosenblatt, J. and Montell, D. J. (2018). Unconventional ways to live and die: cell death and survival in development, homeostasis, and disease. *Annu. Rev. Cell Dev. Biol.* 34, 311-332. doi:10.1146/annurev-cellbio-100616-060748
Hoffmann, R. F., Moshkin, Y. M., Mouton, S., Grzeschik, N. A., Kalicharan, R. D., Kuipers, J., Wolters, A. H. G., Nishida, K., Romashchenko, A. V., Postberg, J. et al. (2016). Guanine quadruplex structures localize to heterochromatin. *Nucleic Acids Res.* 44, 152-163. doi:10.1093/nar/gkv900
Housden, B. E., Lin, S., Perrimon, N. (2014). Cas9–Based genome editing in Drosophila. In *The Use of CRISPR/cas9, ZFNs, TALENs in Generating Site Specific Genome Alterations*, 1st edn (ed. J. A. Doudna and E. J. Sontheimer). Elsevier Inc.
John Peter, A. T., Herrmann, B., Antunes, D., Rapaport, D., Dimmer, K. S. and Kornmann, B. (2017). Vps13-Mcp1 interact at vacuole-mitochondria interfaces and bypass ER-mitochondria contact sites. *J. Cell Biol.* 216, 3219-3229. doi:10.1083/jcb.201610055
Kerr, J. F. R., Wyllie, A. H. and Currie, A. R. (1972). Apoptosis: a basic biological phenomenon with wide-ranging implications in tissue kinetics. *Br. J. Cancer* 26, 239-257. doi:10.1038/bjc.1972.33
Kuipers, J., de Boer, P. and Giepmans, B. N. G. (2015). Scanning EM of non-heavy metal stained biosamples: Large-field of view, high contrast and highly efficient immunolabeling. *Exp. Cell Res.* 337, 202-207. doi:10.1016/j.yexcr.2015.07.012
Kuipers, J., Kalicharan, R. D., Wolters, A. H. G., van Ham, T. J. and Giepmans, B. N. G. (2016). Large-scale scanning transmission electron microscopy (Nanotomy) of healthy and injured zebrafish brain. *J. Vis. Exp.* 25, 53635. doi:10.3791/53635
Kumar, N., Leonzino, M., Hancock-Cerutti, W., Horenkamp, F. A., Li, P., Lees, J. A., Wheeler, H., Reinisch, K. M. and De Camilli, P. (2018). VPS13A and VPS13C are lipid transport proteins differentially localized at ER contact sites. *J. Cell Biol.* 217, 3625-3639. doi:10.1083/jcb.201807019

Lang, A. B., Peter, A. T. J., Walter, P. and Kornmann, B. (2015). ER–mitochondrial junctions can be bypassed by dominant mutations in the endosomal protein Vps13. *J. Cell Biol.* 210, 883-890. doi:10.1083/jcb.201502105
Li, P. Q., Lees, J. A., Lusk, C. P. and Reinisch, K. M. (2020). Cryo-EM reconstruction of a VPS13 fragment reveals a long groove to channel lipids between membranes. *J. Cell Biol.* 219, e202001161. doi:10.1083/jcb.202001161
Mazzalupo, S. and Cooley, L. (2006). Illuminating the role of caspases during Drosophila oogenesis. *Cell Death Differ.* 13, 1950-1959. doi:10.1038/sj.cdd.4401892
Mohammadinejad, R., Moosavi, M. A., Tavakol, S., Vardar, D. Ö., Hosseini, A., Rahmati, M., Dini, L., Hussain, S., Mandegary, A. and Klionsky, D. J. (2018). Necrotic, apoptotic and autophagic cell fates triggered by nanoparticles. *Autophagy* 15, 4-33. doi:10.1080/15548627.2018.1509171
Mondragon, A. A., Yalonetskaya, A., Ortega, A. J., Zhang, Y., Naranjo, O., Elguero, J., Chung, W. S. and McCall, K. (2019). Lysosomal machinery drives extracellular acidification to direct non-apoptotic cell death. *Cell Rep.* 27, 11-19.e3. doi:10.1016/j.celrep.2019.03.034
Muñoz-Braceras, S., Calvo, R. and Escalante, R. (2015). TipC and the chorea-acanthocytosis protein VPS13A regulate autophagy in Dictyostelium and human HeLa cells. *Autophagy* 11, 918-927. doi:10.1080/15548627.2015.1034413
Muñoz-Braceras, S., Tornero-Écija, A. R., Vincent, O. and Escalante, R. (2019). VPS13A is closely associated with mitochondria and is required for efficient lysosomal degradation. *Dis. Model. Mech.* 12, dmm036681. doi:10.1242/dmm.036681
Nakanishi, H., Suda, Y. and Neiman, A. M. (2007). Erv14 family cargo receptors are necessary for ER exit during sporulation in Saccharomyces cerevisiae. *J. Cell Sci.* 120, 908-916. doi:10.1242/jcs.03405
Nezis, I., Stravopodis, D. J., Papassideri, I., Robert-Nicoud, M. and Margaritis, L. H. (2000). Stage-specific apoptotic patterns during oogenesis. *Eur. J. Cell Biol.* 79, 610-620. doi:10.1078/0171-9335-00088
Nezis, I. P., Stravopodis, D. J., Margaritis, L. H. and Papassideri, I. S. (2006). Chromatin condensation of ovarian nurse and follicle cells is regulated independently from DNA fragmentation during Drosophila late oogenesis. *Differentiation* 74, 293-304. doi:10.1111/j.1432-0436.2006.00076.x
Nezis, I. P., Shravage, B. V., Sagona, A. P., Lamark, T., Bjørkøy, G., Johansen, T., Rusten, T. E., Brech, A., Baehrecke, E. H. and Stenmark, H. (2010). Autophagic degradation of dBruce controls DNA fragmentation in nurse cells during late Drosophila melanogaster oogenesis. *J. Cell Biol.* 190, 523-531. doi:10.1083/jcb.201002035
Okada, E. and Waddington, C. H. (1959). The submicroscopic structure of the drosophila egg. *Development* 7, 583-597.
Park, J.-S. and Neiman, A. M. (2012). VPS13 regulates membrane morphogenesis during sporulation in Saccharomyces cerevisiae. *J. Cell Sci.* 125, 3004-3011. doi:10.1242/jcs.105114
Park, J.-S., Okumura, Y., Tachikawa, H. and Neiman, A. M. (2013). SPO71 encodes a developmental stage-specific partner for Vps13 in saccharomyces cerevisiae. *Eukaryot. Cell* 12, 1530-1537. doi:10.1128/EC.00239-13
Pérez-Garijo, A., Fuchs, Y. and Steller, H. (2013). Apoptotic cells can induce non-autonomous apoptosis through the TNF pathway. *Elife* 2, e01004. doi:10.7554/eLife.01004
Peterson, J. S. and McCall, K. (2013). Combined inhibition of autophagy and caspases fails to prevent developmental nurse cell death in the Drosophila melanogaster ovary. *PLoS ONE* 8, e76046. doi:10.1371/journal.pone.0076046
Peterson, J. S., Barkett, M. and McCall, K. (2003). Stage-specific regulation of caspase activity in drosophila oogenesis. *Dev. Biol.* 260, 113-123. doi:10.1016/S0012-1606(03)00240-9
Peterson, J. S., Timmons, A. K., Mondragon, A. A., McCall, K. (2015). The end of the beginning. In *Current Topics in Developmental Biology* (ed. H. Steller), pp. 93-119. Elsevier Inc.
Poon, I. K. H., Lucas, C. D., Rossi, A. G. and Ravichandran, K. S. (2014). Apoptotic cell clearance: basic biology and therapeutic potential. *Nat. Rev. Immunol.* 14, 166-180. doi:10.1038/nri3607
Rampoldi, L., Dobson-Stone, C., Rubio, J. P., Danek, A., Chalmers, R. M., Wood, N. W., Verellen, C., Ferrer, X., Malandrini, A., Fabrizi, G. M. et al. (2001). A conserved sorting-associated protein is mutant in chorea-acanthocytosis. *Nat. Genet.* 28, 119-120. doi:10.1038/88821
Riedel, F., Gillingham, A. K., Rosa-Ferreira, C., Galindo, A. and Munro, S. (2016). An antibody toolkit for the study of membrane traffic in Drosophila melanogaster. *Biol. Open* 5, 987-992. doi:10.1242/bio.018937
Sander, J. D. and Joung, J. K. (2014). CRISPR-Cas systems for genome editing, regulation and targeting. *Nat. Biotechnol.* 32, 347-355. doi:10.1038/nbt.2842
Schnell, U., Dijk, F., Sjollema, K. A. and Giepmans, B. N. G. (2012). Immunolabeling artifacts and the need for live-cell imaging. *Nat. Methods* 9, 152-158. doi:10.1038/nmeth.1855
Serizier, S. B. and McCall, K. (2017). Scrambled eggs: apoptotic cell clearance by non-professional phagocytes in the Drosophila ovary. *Front. Immunol.* 8, 1642. doi:10.3389/fimmu.2017.01642
Sokol, E., Kramer, D., Diercks, G. F. H., Kuipers, J., Jonkman, M. F., Pas, H. H. and Giepmans, B. N. G. (2015). Large-scale electron microscopy maps of patient

DEVELOPMENT

14

skin and mucosa provide insight into pathogenesis of blistering diseases. *J. Invest. Dermatol.* **135**, 1763-1770. doi:10.1038/jid.2015.109

**Tait, S. W. G., Ichim, G. and Green, D. R.** (2014). Die another way – non-apoptotic mechanisms of cell death. *J. Cell Sci.* **127**, 2135-2144. doi:10.1242/jcs.093575

**Timmons, A. K., Mondragon, A. A., Schenkel, C. E., Yalonetskaya, A., Taylor, J. D., Moynihan, K. E., Etchegaray, J. I., Meehan, T. L. and McCall, K.** (2016). Phagocytosis genes nonautonomously promote developmental cell death in the Drosophila ovary. *Proc. Natl. Acad. Sci. USA* **113**, E1246-E1255. doi:10.1073/pnas.1522830113

**Timmons, A. K., Mondragon, A. A., Meehan, T. L. and McCall, K.** (2017). Control of non-apoptotic nurse cell death by engulfment genes in Drosophila. *Fly (Austin)* **11**, 104-111. doi:10.1080/19336934.2016.1238993

**Tran, D. H. and Berg, C. A.** (2003). Bullwinkle and shark regulate dorsal-appendage morphogenesis in Drosophila oogenesis. *Development* **130**, 6273-6282. doi:10.1242/dev.00854

**Ueno, S., Maruki, Y., Nakamura, M., Tomemori, Y., Kamae, K., Tanabe, H., Yamashita, Y., Matsuda, S., Kaneko, S. and Sano, A.** (2001). The gene encoding a newly discovered protein, chorein, is mutated in chorea-acanthocytosis. *Nat. Genet.* **28**, 121-122. doi:10.1038/88825

**Verheyen, E. and Cooley, L.** (1994). Looking at oogenesis. *Methods Cell Biol.* **44**, 545-561. doi:10.1016/S0091-679X(08)60931-0

**Vonk, J. J., Yeshaw, W. M., Pinto, F., Faber, A. I. E., Lahaye, L. L., Kanon, B., van der Zwaag, M., Velayos-Baeza, A., Freire, R., van IJzendoorn, S. C. et al.** (2017). Drosophila Vps13 is required for protein homeostasis in the brain. *PLoS ONE* **12**, e0170106. doi:10.1371/journal.pone.0170106

**Wang, Y., Mijares, M., Gall, M. D., Turan, T., Javier, A., Bornemann, D. J., Manage, K. and Warrior, R.** (2010). Drosophila variable nurse cells encodes arrest defective 1 (ARD1), the catalytic subunit of the major N-terminal acetyltransferase complex. *Dev. Dyn* **239**, 2813-2827. doi:10.1002/dvdy.22418

**Wilson, N. S., Dixit, V. and Ashkenazi, A.** (2009). Death receptor signal transducers: nodes of coordination in immune signaling networks. *Nat. Immunol.* **10**, 348-355. doi:10.1038/ni.1714

**Xue, Y., Schmollinger, S., Attar, N., Campos, O. A., Vogelauer, M., Carey, M. F., Merchant, S. S. and Kurdistani, S. K.** (2017). Endoplasmic reticulum–mitochondria junction is required for iron homeostasis. *J. Biol. Chem.* **292**, 13197-13204. doi:10.1074/jbc.M117.784249

**Yalonetskaya, A., Mondragon, A. A., Hintze, Z. J., Holmes, S. and McCall, K.** (2020). Nuclear degradation dynamics in a nonapoptotic programmed cell death. *Cell Death Differ.* **27**, 711-724. doi:10.1038/s41418-019-0382-x

**Yeshaw, W. M., van der Zwaag, M., Pinto, F., Lahaye, L. L., Faber, A. I., Gómez-Sánchez, R., Dolga, A. M., Poland, C., Monaco, A. P., van IJzendoorn, S. C. et al.** (2019). Human VPS13A is associated with multiple organelles and influences mitochondrial morphology and lipid droplet motility. *Elife* **8**, e43561. doi:10.7554/eLife.43561

**Zhu, A. J., Zheng, L., Suyama, K. and Scott, M. P.** (2003). Altered localization of Drosophila smoothened protein activates hedgehog signal transduction. *Genes Dev.* **17**, 1240-1252. doi:10.1101/gad.1080803

# Faber et al., Figure S1



**A**. Schematic representation of the *Vps13* gene showing the target sites of the sgRNAs for the generation of a *Vps13null* mutant using the CRISPR/Cas9 system. Exons are shown as black boxes. Target sites of the qPCR primer set 1 and 2 are indicated. In addition, the localization of the PiggyBac insertion site of the *Vps13PB* mutant is depicted. Sequences of the *Vps13* genomic region are indicated of the control (CC control) strain and the *Vps13null*. The released sequence of the *Vps13* gene (flybase.org) is provided as well as the sequence of exon 8. Antibodies (Vps13NT and Vps13#62) recognize indicated parts of the Vps13 protein.

**Figure S1 –Vps13 gene schematic and validation of the *Vps13null* mutant**

**B.** Egg laying capacity of wild type (*WT), Vps13PB*, *Vps13null* and *Vps13null/Vps13PB* was recorded for 12 days. The total egg production was quantified. For statistical analysis an unpaired student's t-test was used.

**C**. Relative levels of *Vps13* mRNA in the *Vps13null* mutant and the isogenic *CC control* adult flies were determined with RT qPCR using two primer sets (primer set 1 and primer set 2). Data are mean ± SEM, n=3. For statistical analysis an unpaired student's t-test was used.

**D**. Lifespan analysis of the *Vps13PB* and *Vps13null* mutant compared with control flies (*CC control*).

# Faber et al., Figure S2
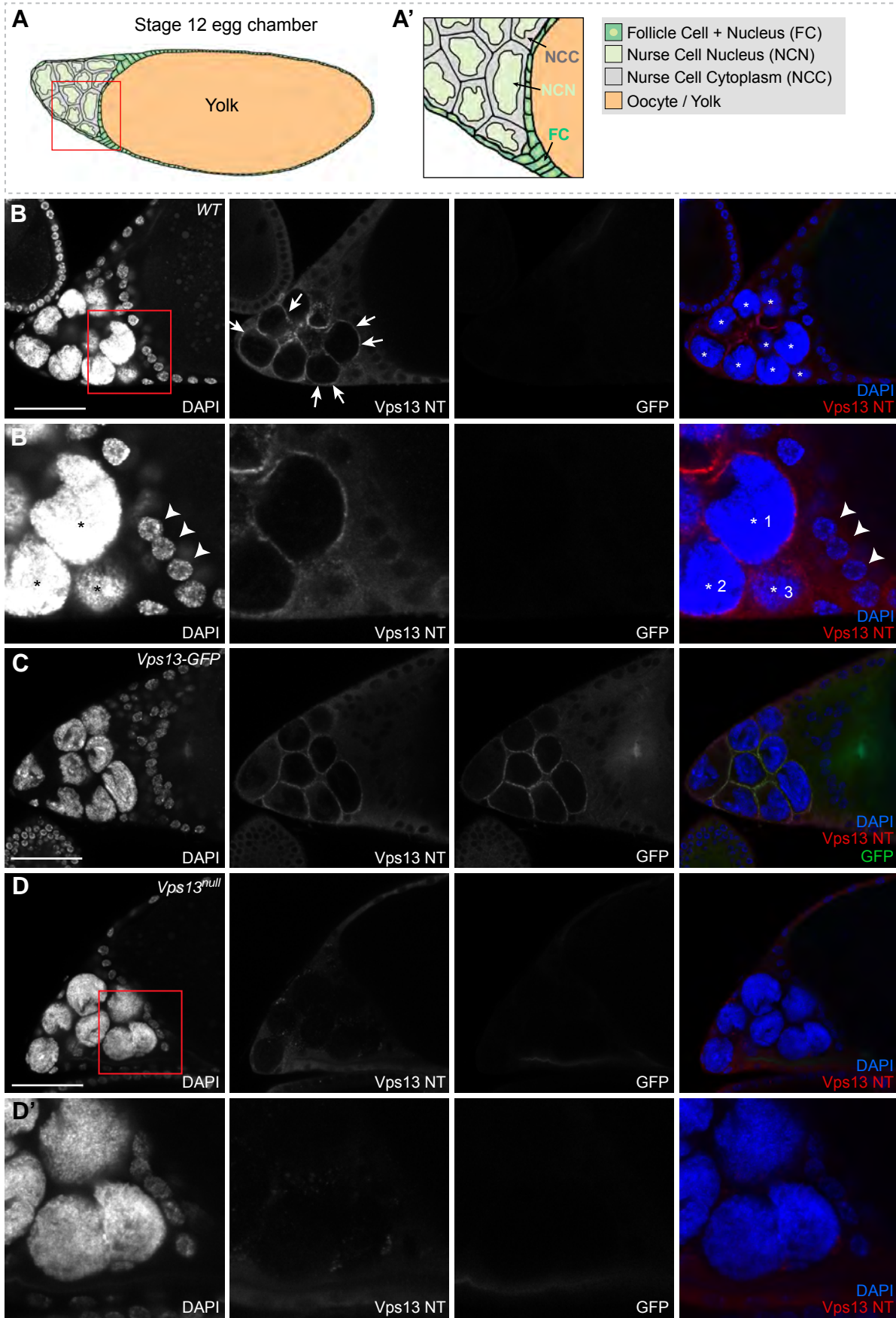
**Figure S2 – Vps13 is expressed during late stages of oogenesis**

**A-A'**. Schematic representations of a stage 12 egg chamber. **A'** is an enlargement of the red box in **A**. **B-D.** Immunolabeling of stage 12 egg chambers from wild type (**B-B'**), the generated *Vps13-GFP* fly line (**C**) and *Vps13$^{null}$* (**D-D'**) flies showing endogenous localization of Vps13 as visualized with the Vps13 NT antibody (red) and the Vps13-GFP fusion protein in the *Vps13-GFP* fly line (green). As an example arrows indicate the Vps13 specific signal in some of the degrading nurse cells. Nuclei of follicle cells are indicated with a white arrowhead, nurse cell nuclei are marked with asterisks. The small nurse cell*$^3$ represents a nurse cell in a more advanced stage of degradation compared to nurse cell*$^1$ and *$^2$ **B'** and **D'** are enlargements of the red boxes in **B** and **D** respectively. Scale bars indicate 50 µm.

# Faber et al., Figure S3
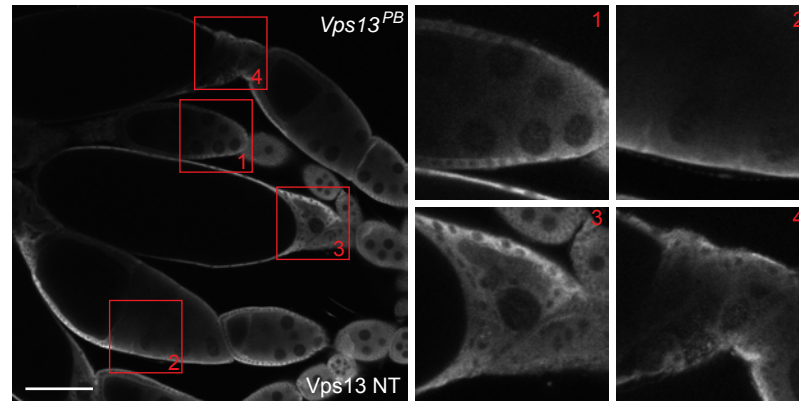


**Figure S3 – Vps13 signal is absent during late stages of oogenesis in $Vps13^{PB}$ mutants**

Ovaries were dissected, fixed and immunolabeled with the Vps13 NT antibody.

Various stages of egg chambers of $Vps13^{PB}$ mutant flies are shown. The boxed areas represent various developmental stages and are enlarged. Box 1 shows an early stage before stage 10. Box 2 shows an egg chamber at stage 10. Box 3 shows an egg chamber at stage 12. Nurse cells at this stage are decreasing in size. Box 4 shows a stage 13 egg chamber, the nurse cells are further degraded and the nurse cell compartment is further decreased in size. Comparable to the $Vps13^{null}$ mutant ovaries, no specific signal is present in $Vps13^{PB}$ mutants. Scale bar indicates 100 µm.

# Faber et al., Figure S4

**A**



sgRNA GFP tag

**B**
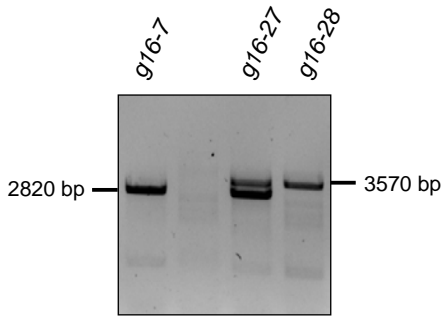


**C**
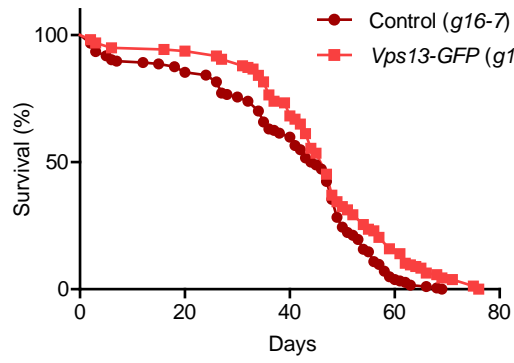


**D**
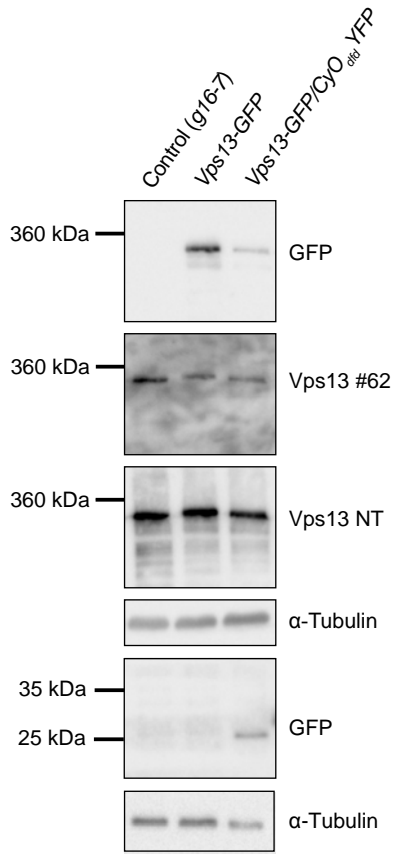


**E**
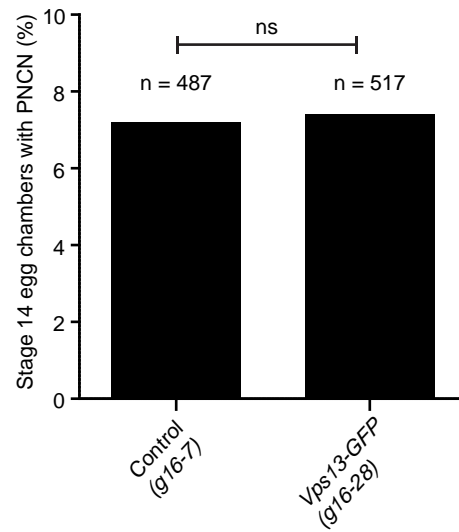
**Figure S4 – Creation and validation of a *Vps13-GFP* fly line using CRISPR/Cas9**

**A**. Schematic representation of the *Vps13* gene showing the target site of the sgRNA for the generation of the *Vps13-GFP* line using the CRISPR/Cas9 system. Exons are shown as black boxes.

**B**. Potential *Vps13-GFP* lines (*g16*-7, *g16-27* and *g16-28*) were screened by PCR amplification of the flanking regions of the *GFP* sequence to confirm the incorporation of the ~750 bp *GFP* sequence. GFP negative lines should give a PCR product of 2820 bp (*g16-7*), while *Vps13-GFP* lines should give a PCR product of 3570 bp (*g16-28*). Heterozygous *Vps13-GFP* flies should show both PCR products (*g16-27*). **C**. Lifespan analysis of the identified *Vps13-GFP* line (*g16-28*) and an isogenic control (*g16-7*) was performed to examine any effects of the inserted *GFP* sequence on viability.

**D**. Western blot analysis of control (*g16-7*), homozygous *Vps13-GFP* and heterozygous *Vps13-GFP/CyO$_{dfd}$YFP* fly heads was performed to visualize the Vps13-GFP fusion protein using a GFP antibody that detects the Vps13-GFP fusion protein in homozygous and heterozygous *Vps13-GFP* flies, but not in the control. Vps13 #62 and Vps13 NT antibodies were used to visualize the Vps13 protein in all samples. Free YFP could only be detected, with the anti-GFP antibody, in heterozygous *Vps13-GFP/CyO$_{dfd}$YFP* lysates because of the YFP-tagged balancer. α-Tubulin was used as a loading control.

**E**. Quantification of persistent nurse cell nuclei in stage 14 egg chambers of 4 day old *Vps13-GFP* and control (*g16-7*) females was performed to test functionality of the Vps13-GFP fusion protein in the *Drosophila* ovary and shows the absence of the *Vps13* mutant ovary phenotype of PNCN accumulation in the newly generated *Vps13-GFP* fly line. Statistical analysis was carried out using Fisher's exact test.

# Faber et al., Figure S5
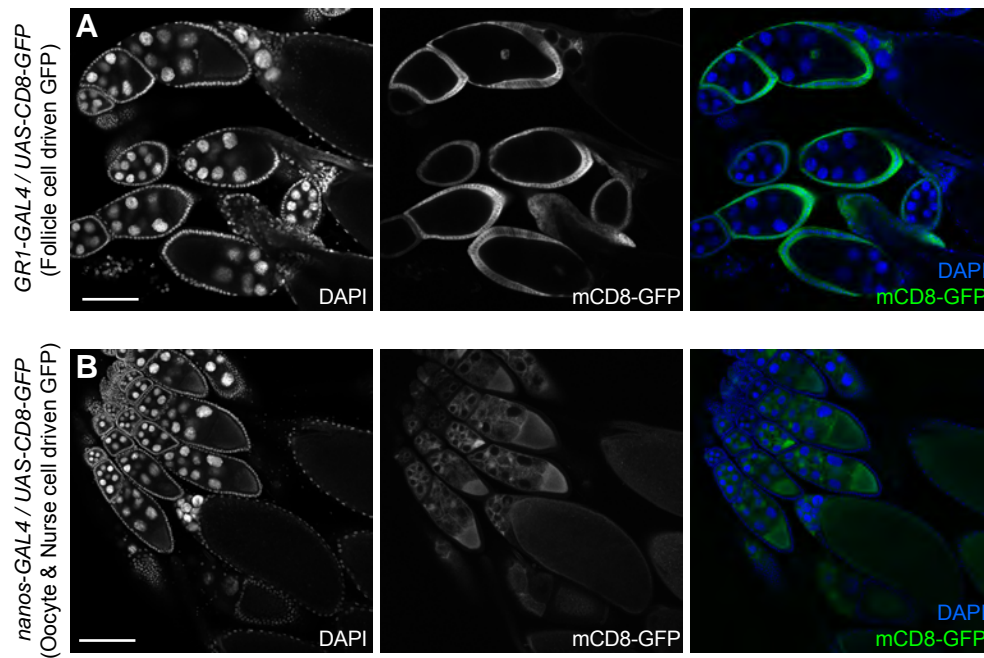


**Figure S5 – Validation of *Vps13 RNAi* in germline cells and follicle cells**

**A-B.** Overview of the expression patterns of the follicle cell driver *GR1-GAL4* (**A**) and nurse cell driver *nanos-GAL4* (**B**) driving *UAS-mCD8-GFP* (green) in *Drosophila* ovaries showing that expression of mCD8-GFP is limited to the cell types in which GAL4 is active. DAPI was used to visualize DNA (blue). Scale bars represent 50 µm.

# Faber et al., Figure S6
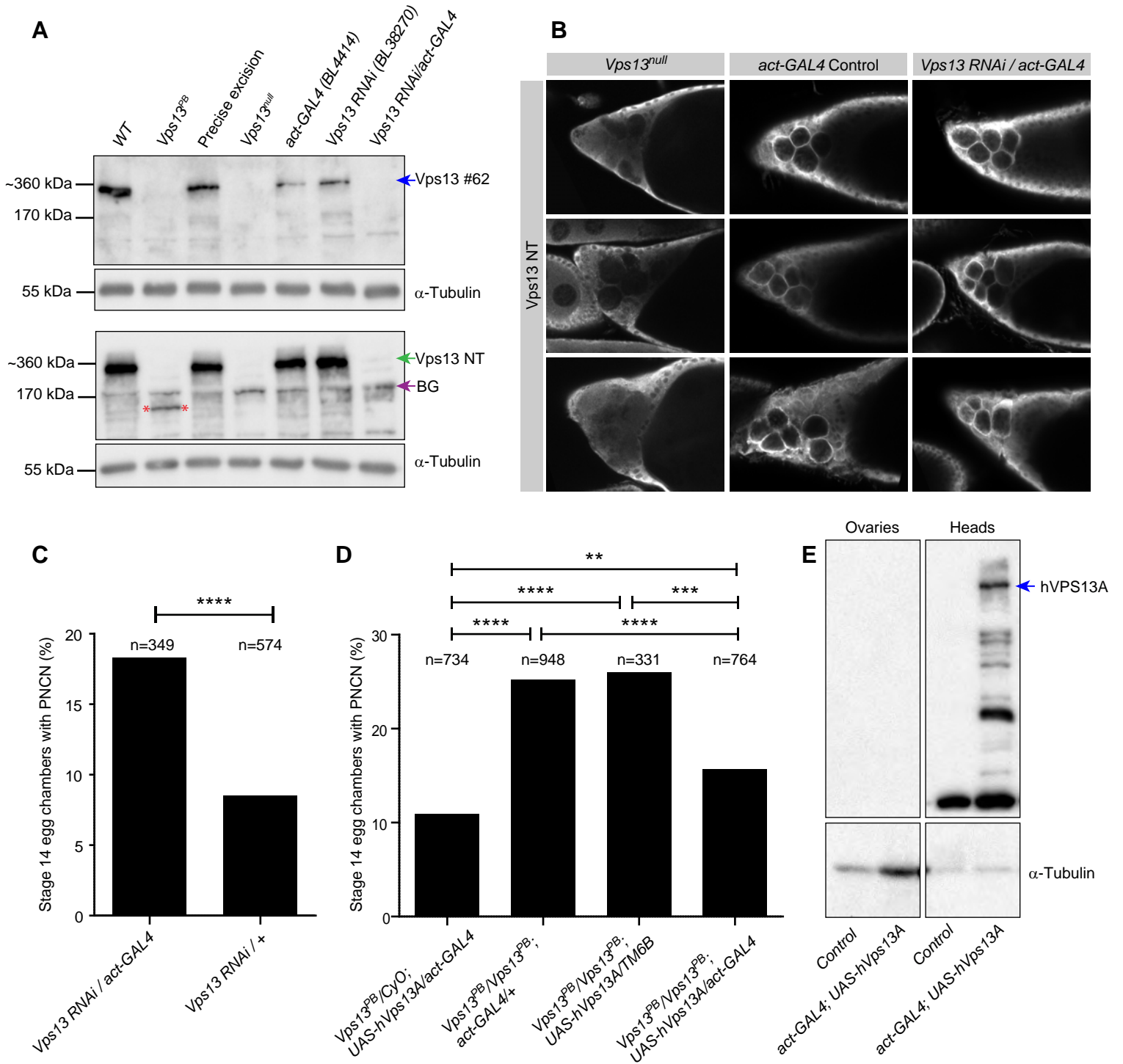
**Figure S6 – Validation of ubiquitous Vps13 RNAi expression**

**A.** To test the efficiency of the *Vps13 RNAi*, Vps13 protein levels were analyzed using Western blot in fly head samples of *Vps13 RNAi/act-GAL4* and control (*4414* and *Vps13 RNAi*). In addition, fly head samples of *WT,* precise excision, $Vps13^{null}$ and $Vps13^{PB}$ mutant lines were loaded. Vps13 levels were detected with both the Vps13 #62 (CT) and Vps13 NT antibody. α-Tubulin was used as a loading control. Arrows indicate the band migrating around 360 kDa, representing the Vps13 full length protein. Asterisks indicate the truncated Vps13 product, only expressed in the $Vps13^{PB}$ mutant line. BG indicate a background band, present in all samples detected by the Vps13 NT antibody.

**B.** Ovaries of control (*act-GAL4/+*), *Vps13 RNAi/act-GAL4* and the $Vps13^{null}$ mutant were dissected, fixed and stained with the Vps13 NT antibody. The specific Vps13 signal is visible in control ovaries and in *act-GAL4/Vps13 RNAi* egg chambers, but not in the $Vps13^{null}$ egg chambers.

**C**. As in Fig. **2C**. Quantification of the percentage of stage 14 egg chambers containing PNCN in *Vps13 RNAi/+* (control) ovaries and *act-GAL4/Vps13 RNAi* (ubiquitous downregulation of Vps13) flies. Statistical analysis was carried out using Fisher's exact test.

**D.** As in Fig. 2C. Quantification of the percentage of stage 14 egg chambers containing PNCN in *Vps13PB/CyO; UAS-hVPS13A/act-GAL4* (control flies), $Vps13^{PB}/Vps13^{PB}$; *act-GAL4/+* ($Vps13^{PB}$ mutant background without human VPS13A expression), $Vps13^{PB}/Vps13^{PB}$; *UAS-hVPS13A/TM6B* ($Vps13^{PB}$ mutant background without human VPS13A expression), $Vps13^{PB}/Vps13^{PB}$; *UAS-hVPS13A/act-GAL4* ($Vps13^{PB}$ mutant background with ubiquitous human VPS13A expression). Statistical analysis was carried out using Fisher's exact test.

**E.** Human VPS13A was ubiquitous expressed using the *act-GAL4* driver, samples of flyheads and ovaries were analysed using Western Blot analysis. An antibody against human VPS13A was used to detect the presence of human VPS13A in the transgenic flies. Human VPS13A was below detection level in the ovary samples. Human VPS13A was detected in Fly heads.
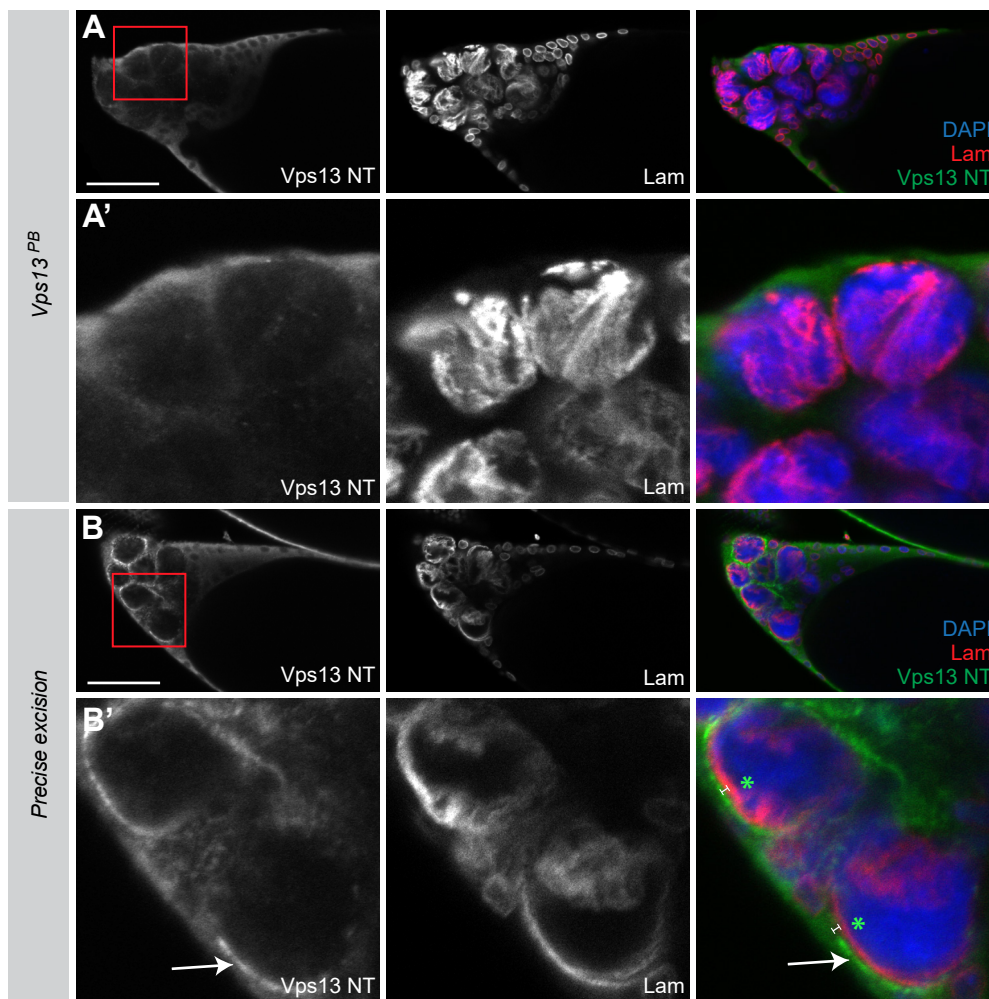
# Faber et al., Figure S7
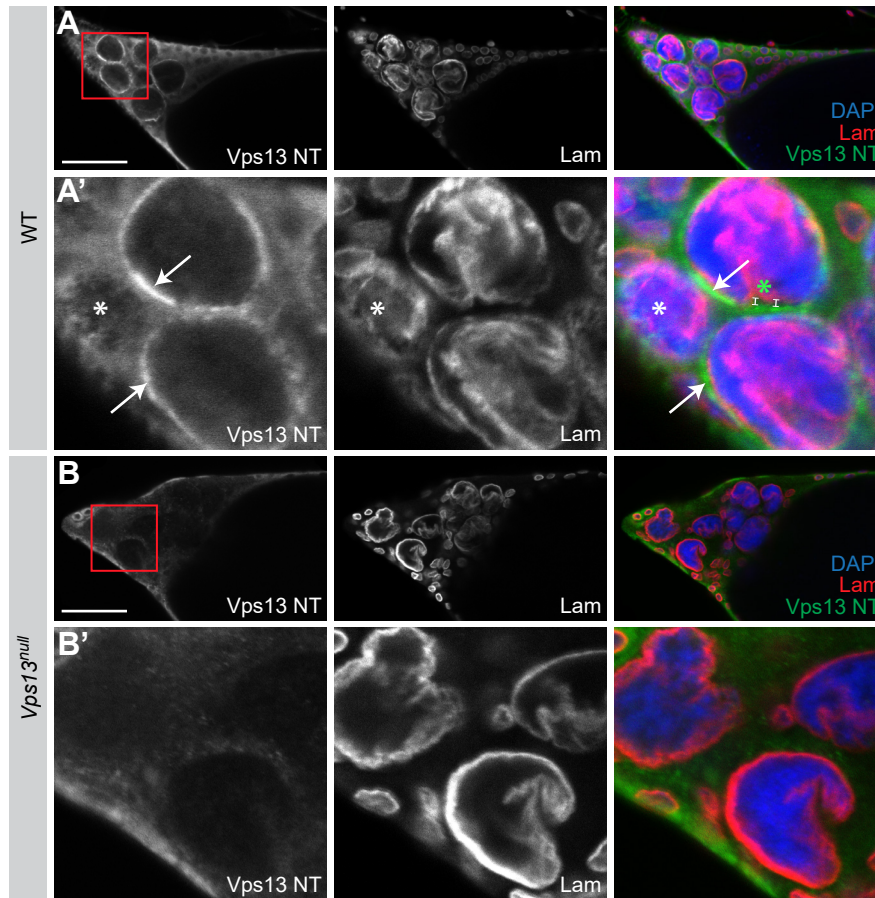


**Figure S7 – Nuclear envelope invaginations occur normally in *Vps13^null^* mutants and Vps13 does not co-localize to the nuclear envelope**

**A-B.** Stage 12 egg chambers of *WT* (**A**) and *Vps13^null^* (**B**) stained with Lamin (Lam, red) to visualize the nuclear envelope, DAPI to visualize DNA and with Vps13 NT antibody (green) to visualize localization of Vps13. In wild type and *Vps13* mutants nuclear envelope invaginations are visible. The panels in **A'-B'** are further enlarged pictures of A-B to illustrate that Vps13 NT and Lamin are in close association, but do not co-localize. An intense Vps13 signal is found when the nuclear envelope and Lamin are still intact, indicated with white arrows. A selection of gaps between the Lamin and Vps13 signal are indicated with green asterisks. Nurse cells in a more advanced stage of degradation, characterized by degradation of the nuclear envelope (indicated by a white asterisk), show decreased Vps13 staining. Scale bars represent 50 μm.

# Faber et al., Figure S8



**Figure S8 – Nuclear envelope invaginations occur normally in *Vps13^BP* mutants and Vps13 is closely associated with but does not co-localize to the nuclear envelope**

**A-B.** Stage 12 egg chambers of *Vps13^PB* (**A-A'**) and the precise excision line (**B-B'**) stained with Lamin (Lam, red) to visualize the nuclear envelope, DAPI to visualize DNA and with Vps13 NT antibody (green) to visualize localization of Vps13. In both the control precise excision line and *Vps13^BP* mutant nuclear envelope invaginations are visible. The panels in A'-B' are further enlarged pictures of A-B to illustrate that Vps13 NT and Lamin are in close association, but do not co-localize. An intense Vps13 signal is found when the nuclear envelope and Lamin are still intact, indicated with white arrows. A selection of gaps between the Lamin and Vps13 signal are indicated with green asterisks. Scale bars represent 50 μm.

# Faber et al., Figure S9
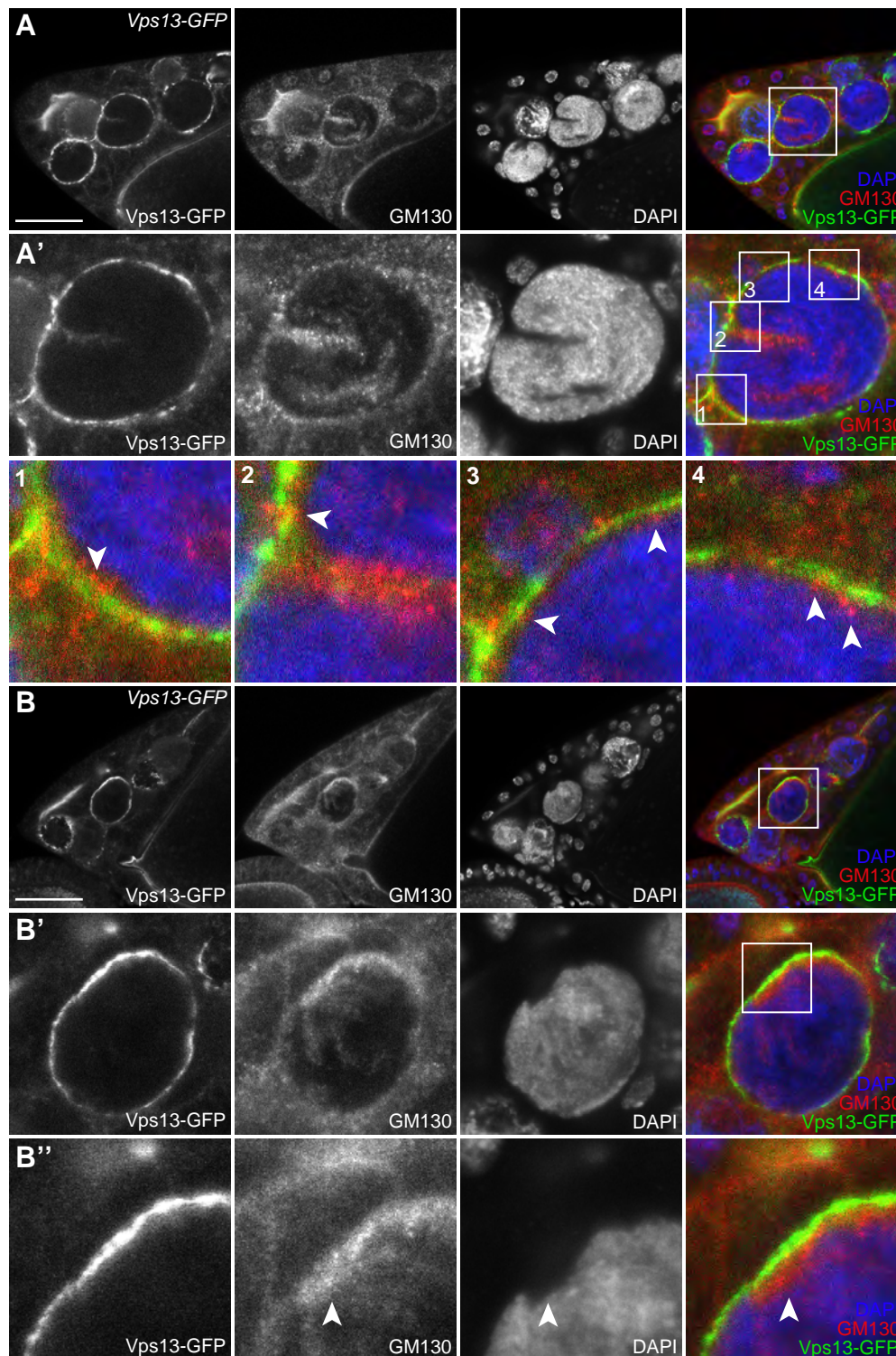


**Figure S9 – Vps13 does not co-localize with the Golgi.**

**A-B.** The Vps13-GFP (in green) expressing line was used to visualize Vps13 expression. GM130 (in red) was used as a marker to visualize localization pattern of Golgi structures, DAPI (in blue) was used to visualize nuclei. Overlays visualize all 3 markers. A and B are representative examples of stage 12 egg chambers. Boxed areas are enlarged in subsequent panels. Arrow heads indicate areas positive for the Golgi marker GM130. The indicated signal does not co-localize with the Vps13-GFP positive signal. Scale bars represent 50 μm.

# Faber et al., Figure S10
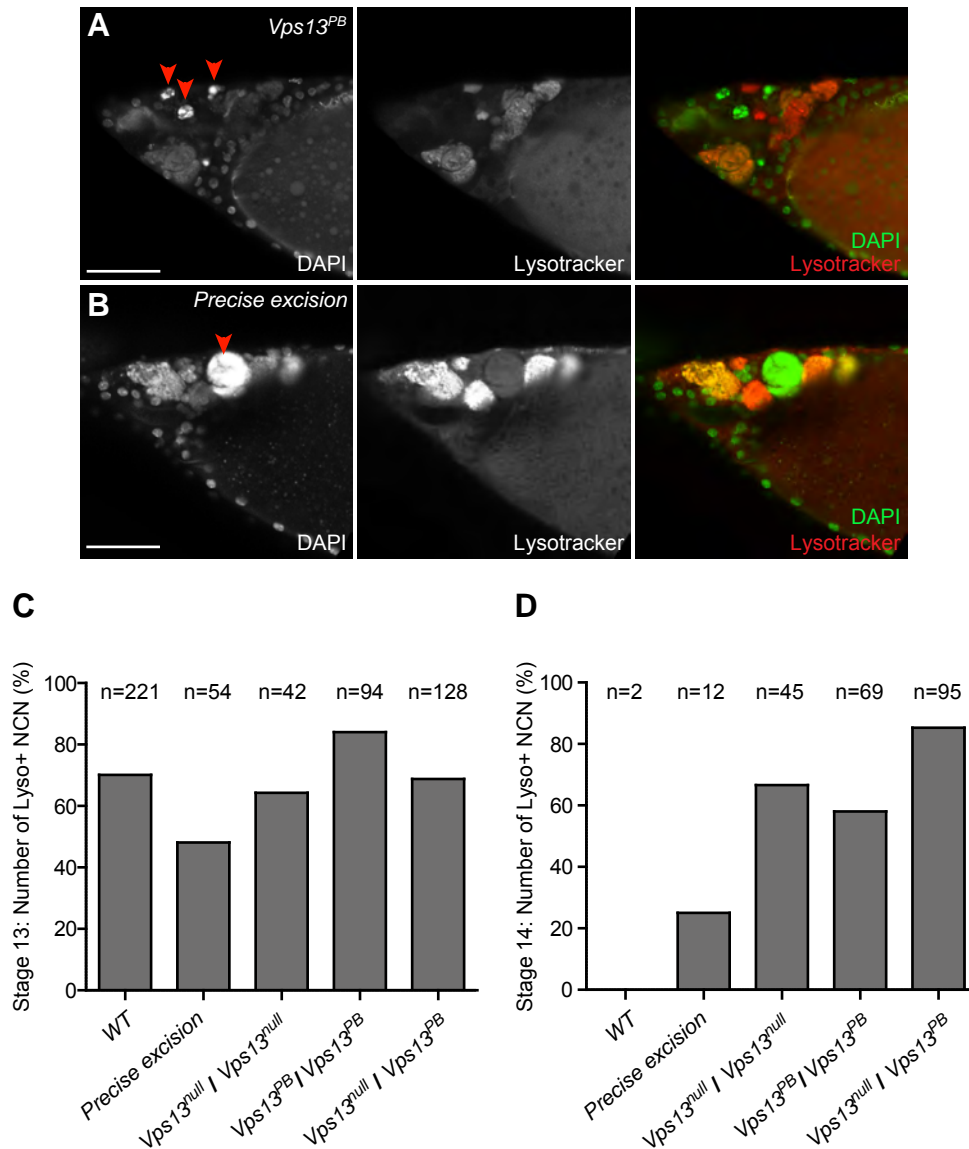


**Figure S10 – Nurse cell acidification during developmental PCD is not affected in *Vps13PB* mutants**

**A-B.** Stage 12 egg chambers of *Vps13BP* (**A**) and the precise excision line (**B**) were labeled with DAPI (green) and Lysotracker (red) to visualize acidification of nurse cell nuclei. Scale bars indicate 50 µm. Degrading pyknotic nurse nuclei are indicated with red arrowheads.

**C.** Percentage of Lysotracker positive nuclei in stage 13 egg chambers was determined in the control (WT, precise excision line) and in *Vps13* (homozygous *Vps13null*, homozygous *Vps13PB*, transheterozygous *Vps13null*/*Vps13PB*) mutant background. Data are consistent with previously published results (Mondragon et al., 2019), demonstrating that at stage 13 around 50 % of all nurse cells are acidified. Number of scored nuclei in stage 13 egg chambers per genotype is indicated.

**D.** Percentage of Lysotracker positive nurse cell nuclei in stage 14 egg chambers was determined in the control (WT, precise excision line) and in *Vps13* (homozygous *Vps13null*, homozygous *Vps13PB*, transheterozygous *Vps13null*/*Vps13PB*) mutant backgrounds. Number of scored PNCN in stage 14 egg chambers is provided per genotype.

# Faber et al., Figure S11
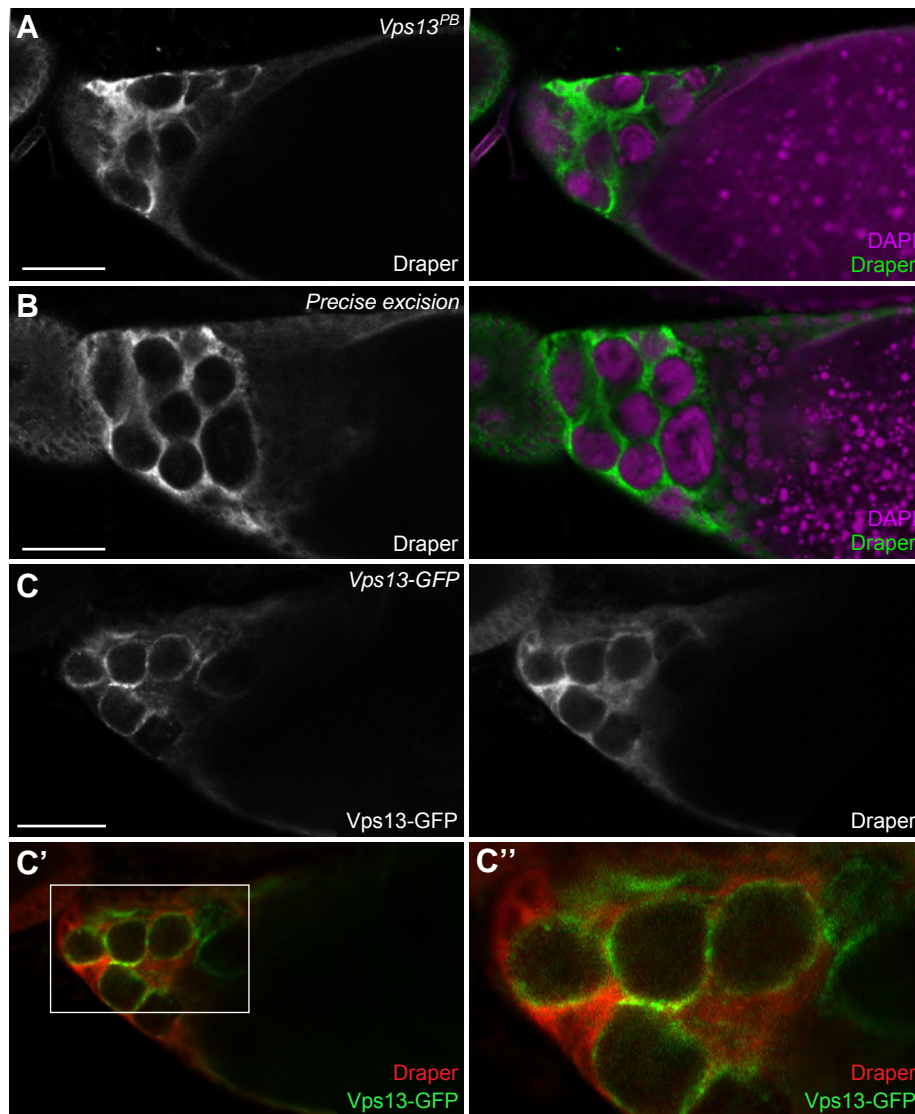


**Figure S11 – Absence of Vps13 does not affect Draper intensity and localization and absence of Draper does not affect Vps13 intensity and localization in ovaries during late stages of oogenesis**

**A-B**. Immunolabeling of stage 12 egg chambers with a Draper specific antibody (green) in *Vps13$^{PB}$* mutants (**A**) and the precise excision line (**B**). DAPI (magenta) was used to visualize nuclei.

**C-C'**. Stage 12 *Vps13-GFP* egg chambers to visualize Draper with a Draper antibody (red) and Vps13 localization by Vps13-GPF (green). The boxed region represents the enlargement shown in **C'**. Scale bars indicate 50 µm.

# Faber et al., Figure S12
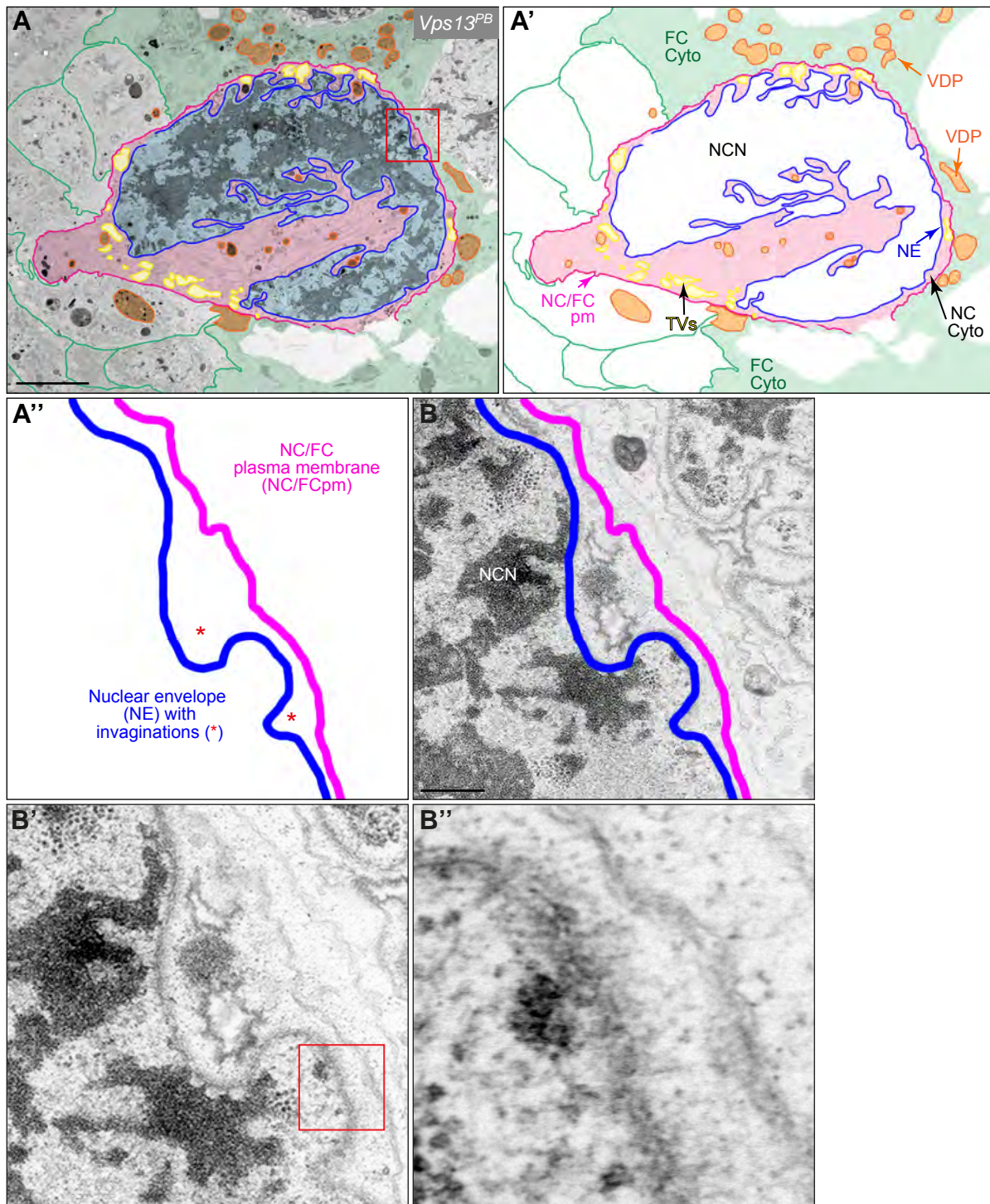
**Figure S12 – Absence of membrane structure associated with the plasma membrane in *Vps13* mutants**

Ultrastructural analysis (**as in Figure 8, 9**) of egg chambers of the *Vps13^PB* mutant.

**A**. Large scale electron microscopic image of the selected region, containing nurse cells and follicle cells. Artificial colors were used to indicate engulfing follicle cells (green), nurse cell cytoplasm (in light magenta), nurse cell nucleus (in blue), translucent vacuoles (in yellow) and vesicles representative for the degradative machinery (in orange). **A'**. Schematic containing structures visible in A. The magenta line indicates the sites of close contact between the plasma membrane of the nurse cell and the plasma membrane of the follicle cell (NC/FCpm), the yellow line indicates the nuclear envelope (NE). NC Cyto=cytoplasm of nurse cells, FC Cyto= cytoplasm of stretch follicle cells, VDP=vesicles representing degradative machinery, TV's=translucent vacuoles.

**B-B'**. Increased zoom in of the area presented in **A"** with (**B**) and without (**B'**) the artificial colors. **B"** is enlargement of the boxed area in **A'**. No membranous structure localized in close association with the plasma membrane was observed. Open access link (www.nanotomy.org). Scale bar in **A** indicates: 5 µm, in **B/B'**: 500 nm.

# Faber et al., Figure S13



Plasma Membrane / Nuclear Envelope / Vps13-dependent Membrane Structure
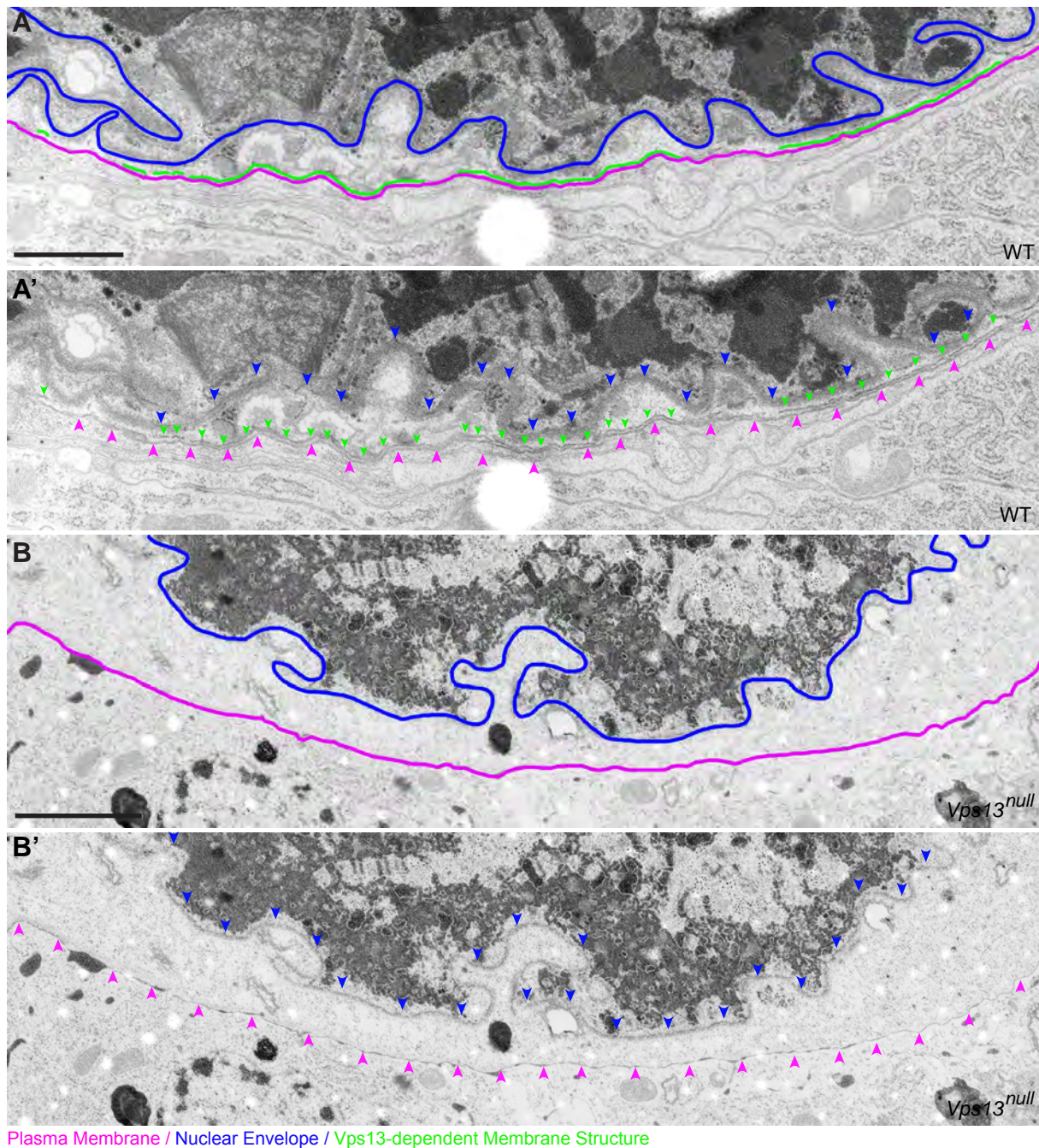
**Figure S13 – Absence of membrane structure associated with the plasma membrane in *Vps13* mutants**

**A-B**. Ultrastructural analysis (**as in Figure 8, 9**) of additional independently prepared egg chambers of the WT control (**A-A'**) and the *Vps13*[null] mutant (**B-B'**). Regions were selected showing part of the degrading nucleus, the nuclear envelope (in blue), the NC/FCpm in magenta and the Vps13-dependent membrane structure in green. Blue arrowheads indicate the nuclear envelope, pink arrowheads the NC/FCpm and green arrowheads the Vps13-dependent structure. Scale bar indicates 1 μm.

# Faber et al., Figure S14



Plasma Membrane / Nuclear Envelope / Vps13-dependent Membrane Structure
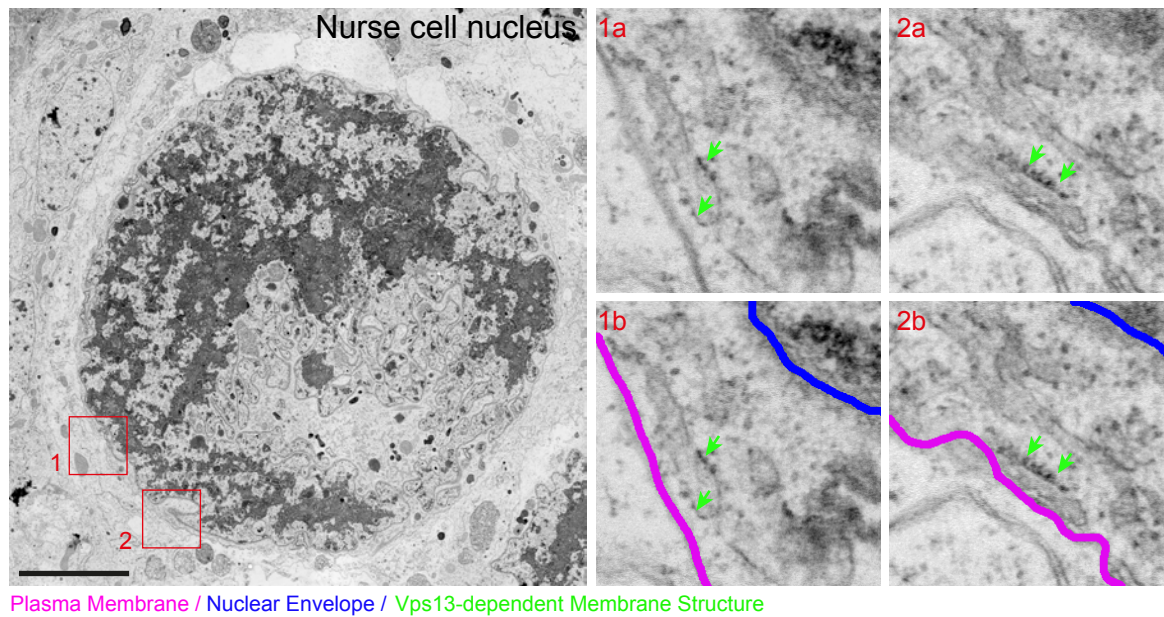
**Figure S14. Structures reminiscent of ribosomes are present on the Vps13-dependent membrane structure.**

**A.** Regions of the WT nucleus represented in **Figure 8** are enlarged visualizing area's in which ribosome-like structures are present on the Vps13-dependent structure. Green arrows indicate the ribosome-like structures.

Artificial colors were used to indicate the NC/FCpm (magenta) and the blue line indicates the nuclear envelope. Scale bar in **A** indicates: 5 µm.
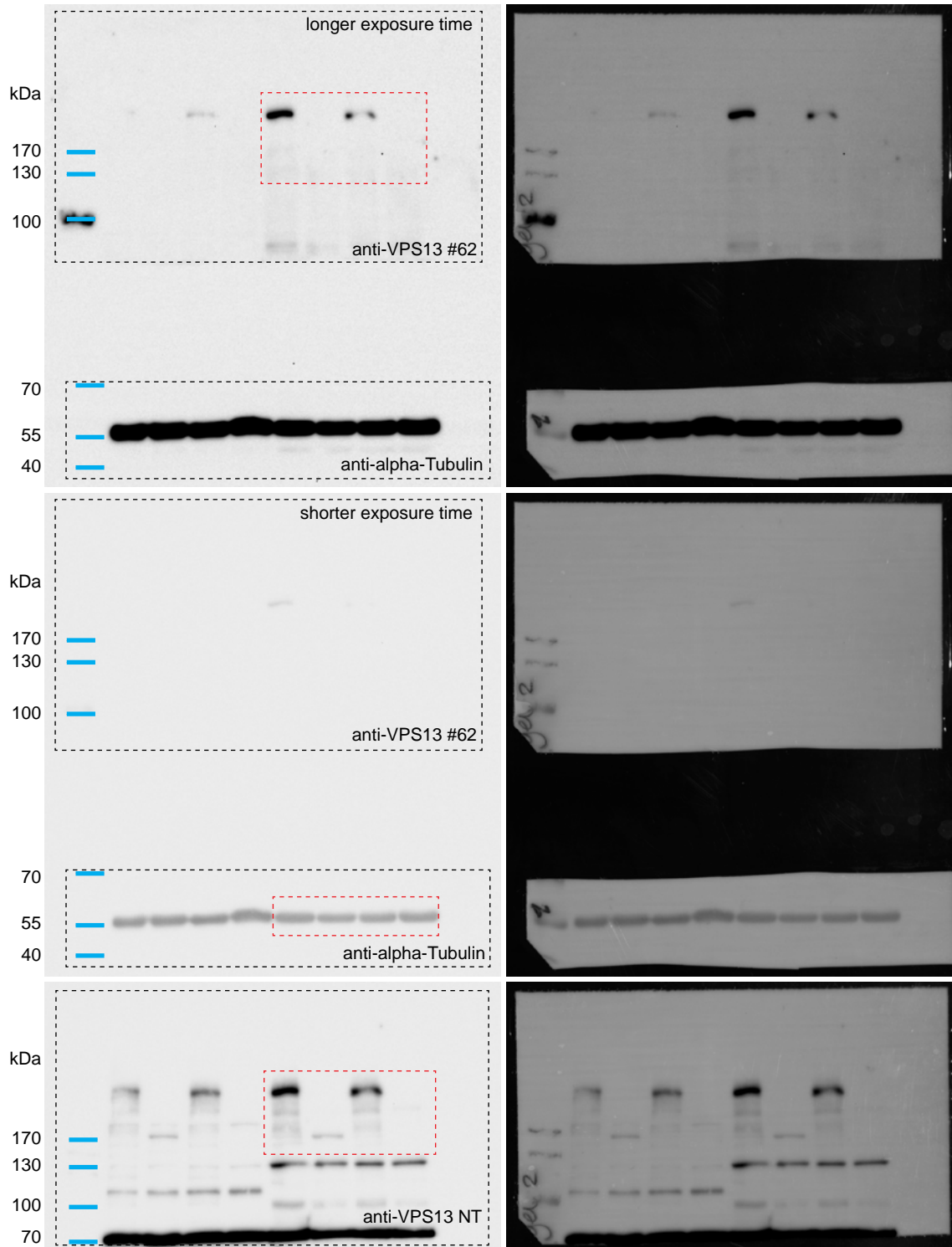
# Faber et al., Figure S15
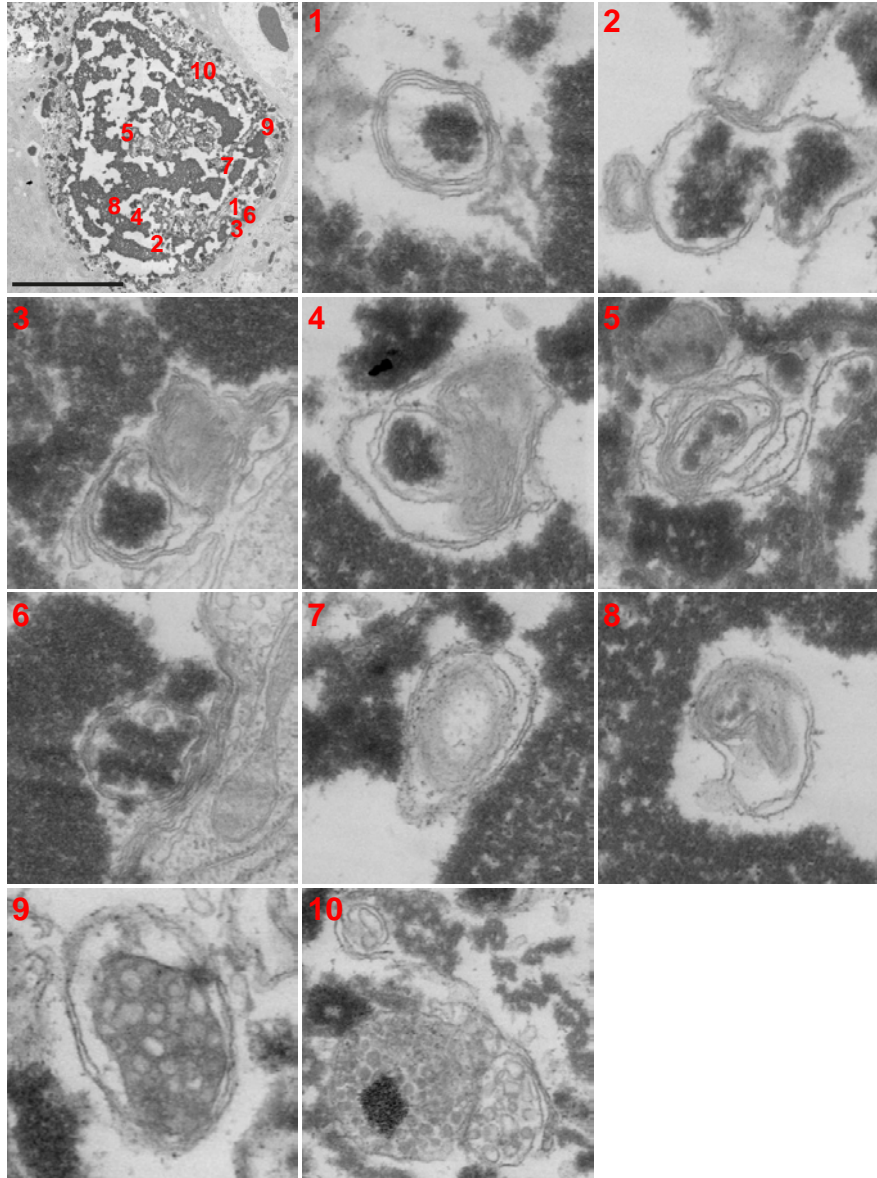


**Figure S15 - membrane structures are visible in degradative nuclei encapsulating chromatin.**

Ultrastructural analysis (**as in Figure 8, 9**) of late stage-13 WT control egg chambers. Stages are chosen containing remnants of nuclei in which the nuclear envelope, plasma membrane and cell boundaries are absent. The chromatin is dispersed and numerous membranous structures are present, including membranes which contain chromatin, multi vesicular bodies, multi laminar bodies. Scale bar indicates 10 μm.
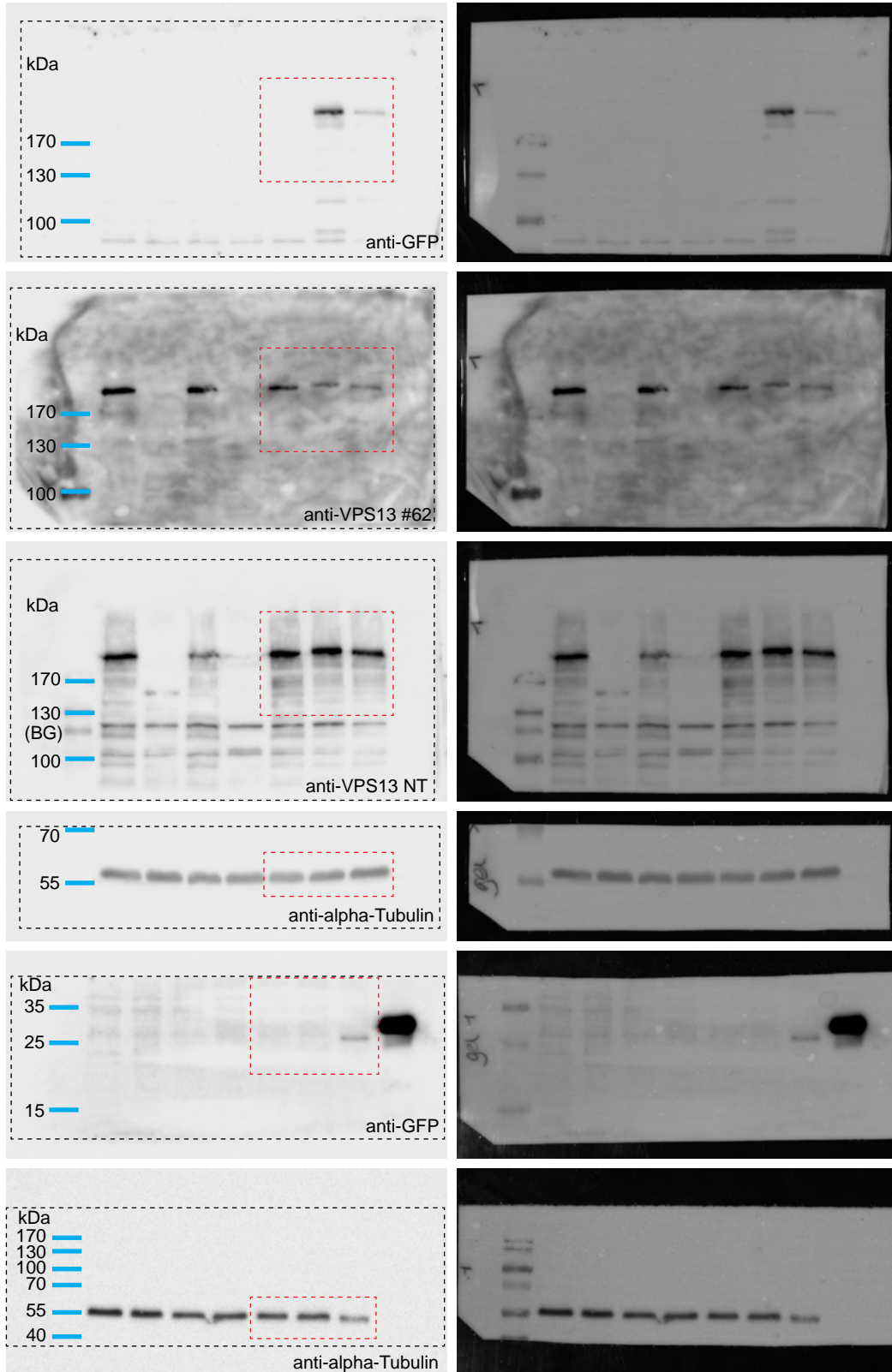
# Faber et al., Figure S16

Original blots used for Figure 1F
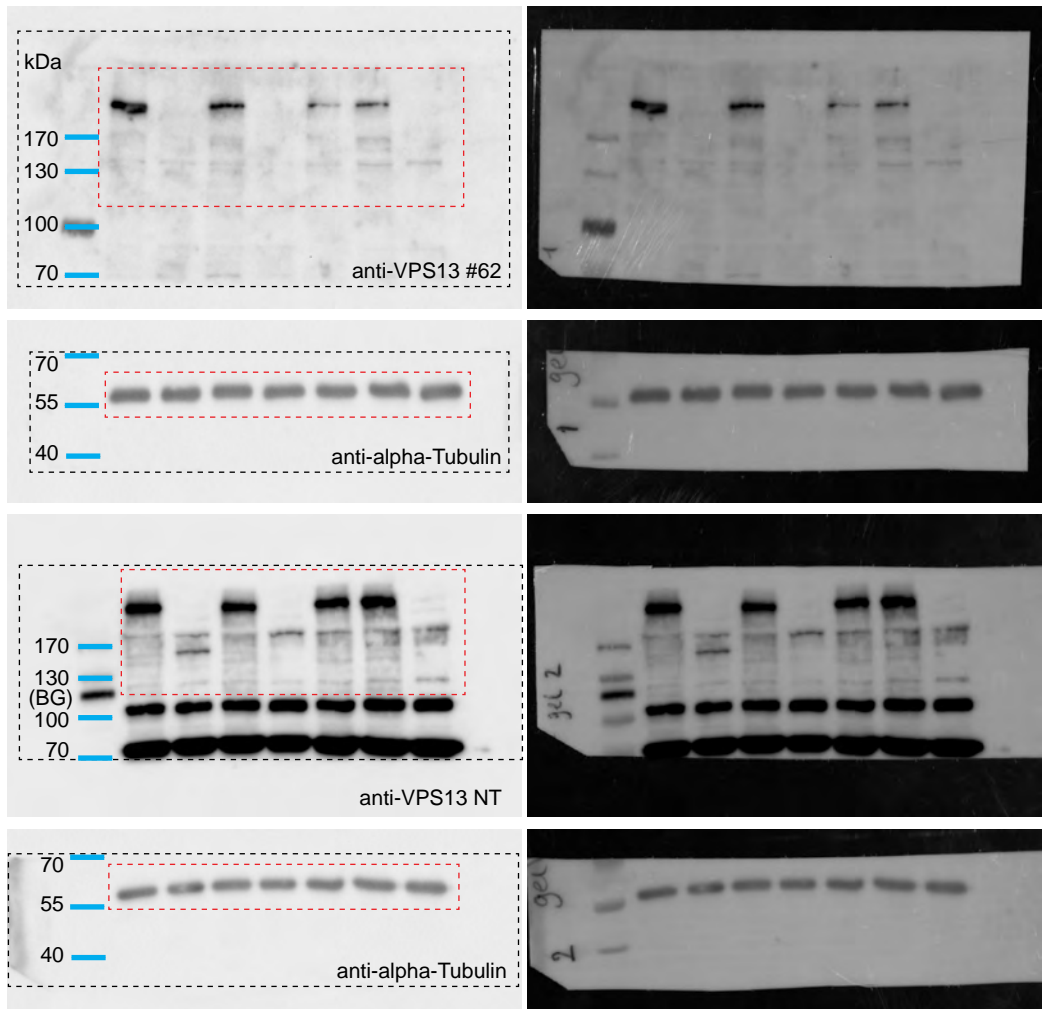
# Faber et al., Figure S17

Original blots used for Figure S4D

# Faber et al., Figure S18

Original blots used for Figure S6A
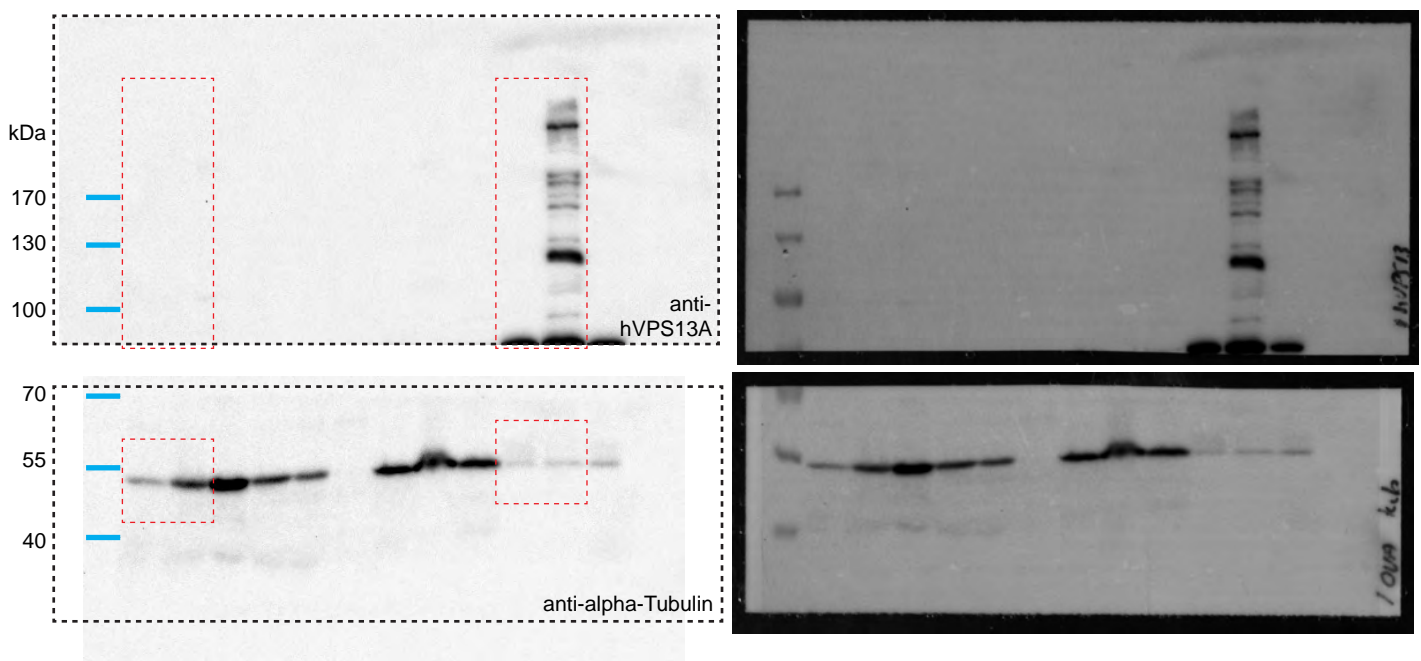


Original blots used for Figure S6E



**Figure S16-S18 –Full scans of indicated Western blots.**

**Table S1. Primers gRNA for Vps13 knockout mutant and Vps13-GFP flies**

| Name | Forward primer | Reverse primer |
|---|---|---|
| sgRNA Exon 4 | CTTCGAAGGGACTACCCGTCGTTG | AAACCAACGACGGGTAGTCCCTTC |
| sgRNA Exon 8 | CTTCGTATGATGCGCCAACCATAT | AAACATATGGTTGGCGCATCATAC |
| sgRNA GFP tag | CTTCGATTATGAGCCGGATAGGCGA | AAACTCGCCTATCCGGCTCATAATC |

**Table S2. Primers HDR donor plasmid**

| Name | Forward primer | Reverse primer |
|---|---|---|
| 5' flanking arm | GCTCCACCGCGGTGGCCAATCCCTATGG CCTAGTGG | ATTATGAGCCGGATAGGCGACTGTAGCCCTTAA CGGATTG |
| GFP sequence | GGCGGCGGCCAATAGAACTGAATTTATT TCCCAAC | GAGGTCGACGGTATCGATAAGCTTGATCCGTGT ATGGTCTCATAGACTC |
| 3' flanking arm | CTATCCGGCTCATAATGCCGCCGCCAGC AAGGGCGAGGAGCTGTTCAC | GGGAAATAAATTCAGTTCTATTGGCCGCCGCCT TACTTGTACAGCTCGTCCAT |

**Table S3. Primers qPCR of new Vps13$^{null}$ mutant**

| Name | Forward primer | Reverse primer |
|---|---|---|
| Primer set 1 | GCGAACGCCAGATTGTTTGA | CAAGACGACATCGCCTCCC |
| Primer set 2 | AGACGTGCCTGGGTCTAT | AAGGCTCGTGAGAGGTAC |
| RP49 | CCGCTTCAAGGGACAGTATC | GACAATCTCCTTGCGCTTCT |

**Table S4. Primers PCR screening of potential Vps13-GFP lines**

| Name | Forward primer | Reverse primer |
|---|---|---|
| GFP | GCCGCCGCCCTTGTACAGCTCGTCCAT | AAGGGCGAGGAGCTGTTCAC |
| GFP + flanking regions | CCTTCTTCGAGCGCGAGTAT | GAAGTTCGTGTACCAGGCCA |